

¹ **The paleogeography of Laurentia in its early years: new
2 constraints from the Paleoproterozoic East-Central
3 Minnesota batholith**

⁴ Nicholas L. Swanson-Hysell¹, Margaret S. Avery¹, Yiming Zhang¹, Eben B.
⁵ Hodgin¹, Robert J. Sherwood¹, Francisco E. Apen², Terrence J. Boerboom³,
⁶ C. Brenhin Keller^{1,4,5}, John M. Cottle²

⁷ ¹Department of Earth and Planetary Science, University of California, Berkeley, CA, USA

⁸ ²Department of Earth Science, University of California, Santa Barbara, CA, USA

⁹ ³Minnesota Geological Survey, St. Paul, MN, USA

¹⁰ ⁴Berkeley Geochronology Center, 2455 Ridge Road, Berkeley, CA, USA

¹¹ ⁵Department of Earth Sciences, Dartmouth College, Hanover, NH, USA

¹² **Key Points:**

- ¹³ • A new *ca.* 1780 Ma paleomagnetic pole reconstructs the Superior province of Lau-
rentia to moderately high latitudes
- ¹⁴ • This pole establishes the coherency of the Laurentia craton following Trans-Hudson
orogenesis and supports the NENA connection with Baltica
- ¹⁵ • Paleomagnetic and geologic data from Laurentia strongly support mobile-lid plate
tectonics from 2.2 Ga to the present day
- ¹⁶
- ¹⁷
- ¹⁸

19 **Abstract**

20 The *ca.* 1.83 Ga Trans-Hudson orogeny resulted from collision of an upper plate
 21 consisting of the Hearne, Rae, and Slave provinces with a lower plate consisting of the
 22 Superior province. While the geologic record of *ca.* 1.83 Ga peak metamorphism within
 23 the orogen suggests that these provinces were a single amalgamated craton from this time
 24 onward, a lack of paleomagnetic poles from the Superior province following Trans-Hudson
 25 orogenesis has made this coherency difficult to test. We develop a high-quality paleo-
 26 magnetic pole for northeast-trending diabase dikes of the post-Penokean orogen East-
 27 Central Minnesota Batholith (pole longitude: 265.8°; pole latitude: 20.4°; A₉₅: 4.5°; K:
 28 45.6 N: 23) whose age we constrain to be 1779.1 ± 2.3 Ma (95% CI) with new U-Pb dates.
 29 Demagnetization and low-temperature magnetometry experiments establish dike rema-
 30 nance be held by low-Ti titanomagnetite. Thermochronology data constrain the intru-
 31 sions to have cooled below magnetite blocking temperatures upon initial emplacement
 32 with a mild subsequent thermal history within the stable craton. The similarity of this
 33 new Superior province pole with poles from the Slave and Rae provinces establishes the
 34 coherency of Laurentia following Trans-Hudson orogenesis. This consistency supports
 35 interpretations that older discrepant 2.22 to 1.87 Ga pole positions between the provinces
 36 are the result of differential motion through mobile-lid plate tectonics. The new pole sup-
 37 ports the NENA connection between the Laurentia and Fennoscandia cratons. The pole
 38 can be used to jointly reconstruct these cratons *ca.* 1780 Ma strengthening the paleo-
 39 geographic position of these major constituents of the hypothesized late Paleoprotero-
 40 zoic supercontinent Nuna.

41 **1 Introduction**

42 In the Orosirian Period of the Paleoproterozoic Era, a series of collisional oroge-
 43 nies led to the amalgamation of Archean provinces to form the core of the Laurentia cra-
 44 ton (Fig. 1; Hoffman (1988); Whitmeyer and Karlstrom (2007)). The most significant
 45 of these orogenies was the *ca.* 1850 to 1800 Ma Trans-Hudson orogeny associated with
 46 the collision between the Superior province and the Churchill province which comprised
 47 a composite of the Slave, Hearne and Rae provinces (Fig. 1; Weller and St-Onge (2017)).
 48 The length of the orogen as well as the pressure-temperature of metamorphism within
 49 it are similar to that of continent-continent collision within the Himalayan orogen (Weller
 50 & St-Onge, 2017). The terminal closure of the intervening ocean basin between the Su-

51 perior and composite Slave + Hearne + Rae provinces is interpreted in paleogeographic
 52 models to be associated not only with the assembly of Laurentia, but also with the con-
 53 joining of other continents into the hypothesized supercontinent Nuna (Pehrsson et al.,
 54 2015).

55 The rapid Paleoproterozoic amalgamation of the Laurentia craton led to the large
 56 persistent area of continental lithosphere that would grow further through accretionary
 57 orogenesis subsequently in the Paleoproterozoic Era and through the Mesoproterozoic
 58 Era (Whitmeyer & Karlstrom, 2007). This subsequent orogenesis along the southern to
 59 eastern margin of Laurentia (present-day coordinates) indicates that it was a long-lived
 60 accretionary margin (Karlstrom et al., 2001; Whitmeyer & Karlstrom, 2007). This ac-
 61 cretionary margin has been interpreted to have extended beyond Laurentia and have con-
 62 tinued onto Baltica and Australia (Karlstrom et al., 2001). Based on correlation of Archean
 63 provinces and Paleoproterozoic orogenic belts, Gower et al. (1990) reconstructed Baltica
 64 to Laurentia in a position known as the NENA (northern Europe and North America)
 65 configuration. This reconstruction is compatible with existing paleomagnetic constraints
 66 from *ca.* 1750 to 1270 Ma (Evans & Pisarevsky, 2008) and these conjoined cratons fea-
 67 ture as a major component of the hypothesized Nuna supercontinent (Evans & Mitchell,
 68 2011; Zhang et al., 2012).

69 Additional data that constrain the paleogeographic position of Laurentia from the
 70 time just following the Trans-Hudson orogeny can test the hypothesis of the unity of Lau-
 71 rentia's Archean provinces, establish the position of the newly amalgamated Laurentia,
 72 and thereby enable tests of hypothesized connections with other cratons. This study de-
 73 velops a new paleomagnetic pole for Laurentia from *ca.* 1780 Ma diabase dikes of the
 74 East-Central Minnesota Batholith (ECMB) that provides such constraints.

75 2 Geologic Setting

76 Coeval with collisional orogenesis between the assembling Archean provinces that
 77 formed Laurentia's core was the *ca.* 1860 to 1820 Ma accretionary Penokean orogeny along
 78 the southern margin of the Superior Province (Fig. 1; Schulz and Cannon (2007)). Penokean
 79 orogenesis resulted from island-arc and microcontinent collisions with the Superior Province
 80 that led to metamorphism of Superior Province lithologies and development of a fore-
 81 land basin (Schulz & Cannon, 2007; Holm et al., 2019). Following the Penokean orogeny,

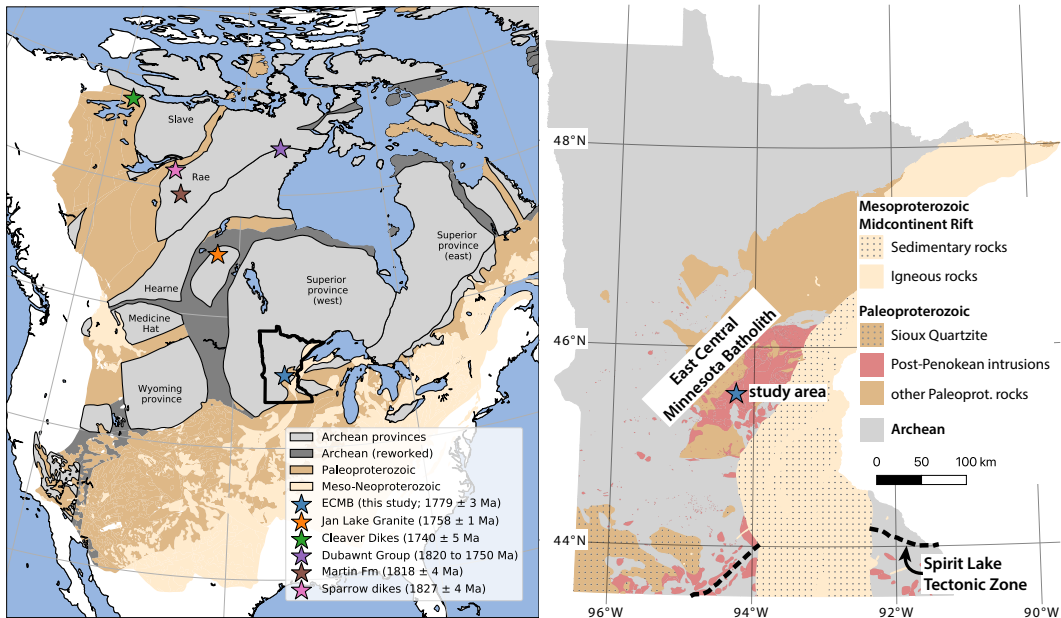


Figure 1. Map of Laurentia showing the location of Archean provinces and younger Proterozoic crust (simplified from Whitmeyer and Karlstrom (2007)). The localities of paleomagnetic poles that constrain Laurentia's position just after its amalgamation are shown with stars including the new pole from this study developed from the East-Central Minnesota Batholith (ECMB). The outline of the state of Minnesota around the ECMB blue star is the region for the geologic map in the right panel. This map shows interpreted Precambrian geology for the state of Minnesota (simplified from Jirsa et al. (2012)) including in regions covered by Phanerozoic sedimentary rocks where the Precambrian bedrock is inferred from geophysical data and drill cores.

there was voluminous magmatism along the southeastern margin of the west Superior Province resulting in the emplacement of the *ca.* 1780 Ma East-Central Minnesota Batholith (ECMB) and other coeval post-orogenic plutons (Fig. 1; Holm et al. (2005); Boerboom et al. (2005); Schmitz et al. (2018)). While the ECMB is dominantly comprised of felsic to intermediate plutons, mafic magmas were also generated and commingled with the more abundant felsic magmas throughout the interval of batholith generation as evidenced by mafic enclaves within some of the plutons (Boerboom et al., 2005, 2011; Schmitz et al., 2018). Mafic melt within the ECMB also led to the emplacement of a set of near-vertical northeast-trending diabase dikes (Fig. 2; Boerboom et al. (2005)). The dikes have chilled margins and are typically 1 to 3 meters wide with widths up to 8 meters (Boerboom et al., 2005). As with the granites they intrude, the dikes have primary igneous texture and no metamorphic fabric (Boerboom et al., 2005). They have experienced variable low-grade alteration such as albitionization and sericitization of plagioclase and the formation

95 of pyrrhotite. These diabase dikes are present within all of the granitoid units of the ECMB
96 (e.g., St. Cloud Granite, Rockville Granite, and Reformatory Granodiorite; Fig. 2) with
97 the exception of the youngest Richmond Granite. Throughout the field area, the dikes
98 are exposed both in glacially-polished pavement outcrops and in numerous inactive and
99 active dimension stone granite quarries. Northeast-trending diabase dikes are present
100 in all of the quarries in the Rockville Granite, St. Cloud Granite as well as in the Re-
101 formatory granodiorite, regardless of the size of the quarry, as well as in many natural
102 bedrock outcrops. In many of the old inactive quarries, the north and/or south quarry
103 walls are marked by the planar surface of a diabase dike contact, where the rock nat-
104 urally separates, often resulting in elongated northeast-southwest shapes to the quarry
105 pits. In contrast, no diabase dikes have been found in the quarries or natural exposures
106 of the Richmond granite. Although this granite does not contain as many quarries and
107 there are fewer natural outcrops, the lack of diabase dikes contrasts sharply with the nu-
108 merous dikes present in the other nearby granites, where an equivalent exposed surface
109 area would contain numerous diabase dikes. This absence indicates that the younger Rich-
110 mond Granite post-dates the intrusion of the diabase dikes into the St. Cloud Granite,
111 Rockville Granite, and Reformatory Granodiorite.

112 There are also quartz-feldspar porphyry dikes with the same northeast-trending di-
113 rection as the diabase dikes found in all the granitoids also with the exception of the Rich-
114 mond Granite (Boerboom et al., 2005). These porphyritic microgranite dikes have chilled,
115 and locally flow-banded, margins. One has been observed to have intruded into a northeast-
116 trending diabase dike and another has textures consistent with commingling of magmas
117 between the felsic dike and adjacent diabase dike indicative of synchronous emplacement
118 (Boerboom & Holm, 2000). The Richmond Granite has trachytoid magmatic fabric de-
119 fined by aligned potassium-feldspar phenocrysts that share the same orientation with
120 the northeast-trending dikes (Boerboom & Holm, 2000), indicating that this orientation
121 is associated with a persistent regional stress field throughout the interval of magma em-
122 placement and dike formation. These field relationships indicate that the quartz-feldspar
123 porphyry and diabase dikes are comagmatic with the batholith. The diabase dikes are
124 constrained to be younger than the St. Cloud Granite (new U-Pb date of 1781.44 ± 0.51
125 Ma; 2σ analytical uncertainty) which they pervasively intrude, older than the Richmond
126 Granite (new U-Pb date of 1776.76 ± 0.49 Ma) in which they are absent, and similar
127 in age to the quartz-feldspar porphyry dikes (new U-Pb date of 1780.78 ± 0.45 Ma).

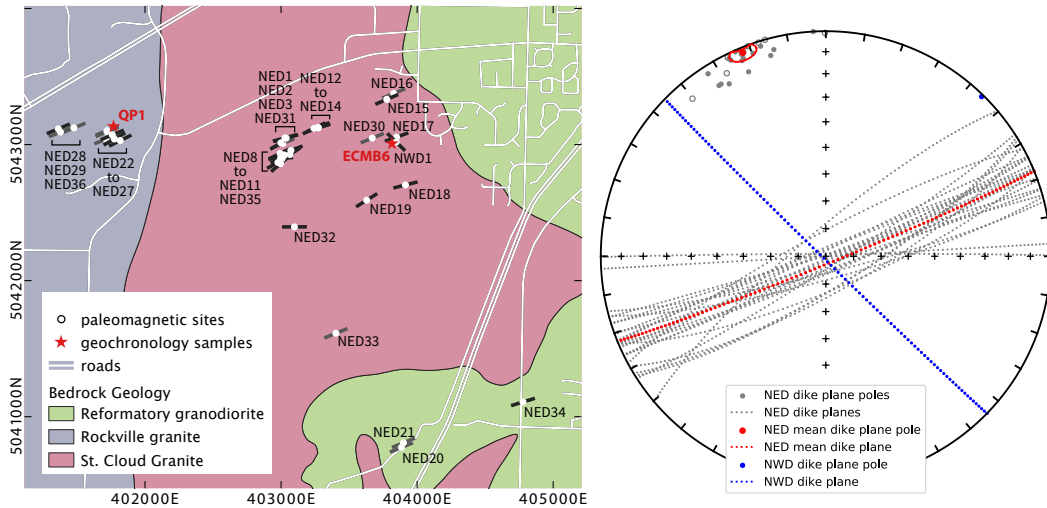


Figure 2. Left panel: Locations of paleomagnetic sites of the northeast-trending dikes (NED) and a northwest-trending dike (NWD) within the Rockville Granite, Reformatory Granodiorite and St. Cloud Granite of the ECMB (bedrock geology from Boerboom et al. (1995) and shown in UTM zone 15N WGS 84 coordinate reference system such that each axis tick is 1 km). Within regions of the mapped St. Cloud Granite there is more complex interfingering of that granite with the Reformatory Granodiorite than is shown. The strikes of the dikes are shown as lines (black when measured on that dike; grey when using the overall mean orientation from the measured NED dikes). The location of the QP1 and ECMB6 geochronology samples are shown. The ECMB4 geochronology sample was collected ~18 km SW of the western edge of the map, in the Richmond Granite which cross-cuts the Rockville Granite and is younger than the NED dikes. Right panel: The orientations of dikes. Each individual dike orientation is the mean of multiple measurements on that dike. The mean of the poles to the NED planes is shown with a red dot and a 95% confidence ellipse on the mean calculated with Fisher statistics. This confidence ellipse intersects the equator indicating that the mean plane cannot be distinguished from vertical.

3 Paleomagnetic Methods and Results

Oriented samples for paleomagnetism were collected and analyzed from 36 of the northeast-trending dikes of the ECMB and one northwest-trending dike (Fig. 2). Each sampled dike constituted a paleomagnetic site in our site naming scheme. These sites were concentrated in and around Stearns County Quarry Park near the city of St. Cloud (Fig. 2). Samples were collected from the dikes with a gas-powered drill and oriented in the field with a Pomeroy orienting fixture. The azimuthal orientations of the cores were determined either through sun or magnetic compass depending on cloud cover. Sun compass directions were preferentially used when available. When magnetic compass data were used they were corrected for local magnetic declination using the International Geomagnetic Reference Field model (Thébault et al., 2015). Specimens from the oriented

samples were analyzed in the UC Berkeley Paleomagnetism lab using a 2G DC-SQUID magnetometer. Samples either underwent stepwise alternating field (AF) or thermal demagnetization. Thermal demagnetization was accomplished using an ASC thermal demagnetizer (residual fields <10 nT). AF demagnetization was conducted with inline coils that utilize a Crest Amplifier paired with an Adwin controller to develop a well-controlled waveform. All paleomagnetic data developed in this study are available at the measurement level in the MagIC database (<https://www.earthref.org/MagIC/> doi/ INSERT-DOI; UPDATE TO DOI WHEN ASSIGNED).

Typical behaviors of sample remanence during demagnetization are illustrated for representative specimens in Figure 3. AF demagnetization data typically reveal three components: a small low-coercivity component approximately aligned with Earth's present local field in the study region that was typically removed below 10 mT; a medium-coercivity component that is steep and was dominantly removed between 10 and 60 mT; and a high-coercivity component that was subsequently removed incompletely as demagnetization progressed to 130 mT. These components are present to varying degrees within individual specimens (Fig. 3).

Sister specimens from some samples underwent thermal and AF demagnetization which provides additional insight into the carriers of the components through comparison of the thermal and AF demagnetization spectra (such as NED2-8 in Fig. 3). These data reveal that the low-coercivity component direction is removed at the lowest unblocking temperatures up to 150°C. This behavior, as well as the typical direction, is most consistent with the component being a viscous overprint acquired in Earth's geomagnetic field. The direction of the high-coercivity component is removed through thermal demagnetization between 250°C and 350°C — consistent with it being held by monoclinic pyrrhotite. The direction of this magnetization held by pyrrhotite is aligned with the magnetite-held remanence within a northwest-trending dike in the region (discussed in more detail below) — a direction consistent with the position of Laurentia during the time period of *ca.* 1096 Ma Midcontinent Rift magmatism (Swanson-Hysell et al., 2020). We interpret this high-coercivity component held by pyrrhotite, whose presence is variable in ECMB dikes, to have formed through hydrothermal activity associated with Midcontinent Rift magmatism such as that represented by the emplacement of the northwest-trending dike. The pyrrhotite thereby carries a chemical remanent magnetization.

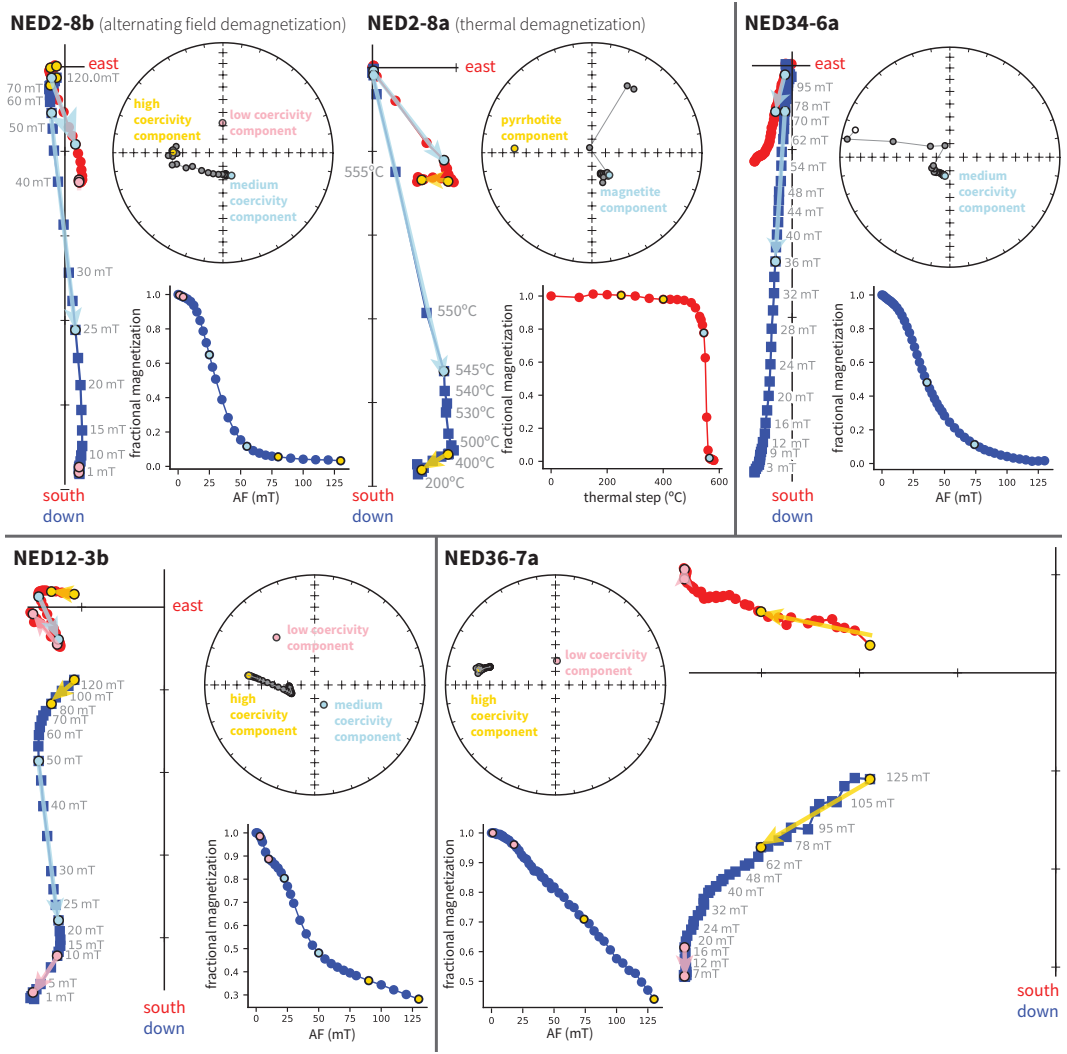


Figure 3. Paleomagnetic data from ECMB northeast-trending diabase dikes are shown in geographic coordinates on vector component plots, measurement-level equal area plots and magnetization magnitude plots (developed using PmagPy software; Tauxe et al. (2016)). Least-squares fits to the data are shown with colored arrows on the vector component plots, colored directions on the equal area plots, and as colored end-points on the magnetization magnitude plots (pink for low-coercivity; blue for medium-coercivity; yellow for high-coercivity). Specimens NED2-8a and NED2-8b are from the same core sample and were analyzed via thermal and alternating field (AF) demagnetization respectively. These data from sample NED2-8 reveal the steep medium-coercivity component to thermally unblock at temperatures characteristic of remanence held by magnetite and the high-coercivity component to thermally unblock at temperatures characteristic of pyrrhotite. Specimen NED34-6a is dominated by the steep medium-coercivity component. The medium-coercivity component is well-resolved in specimen NED12-3b which also has a substantial high-coercivity component. The high-coercivity component dominates the remanence of specimen NED36-7a such that no medium-coercivity component can be resolved.

171 In some specimens, the low-coercivity component is much larger and has a direc-
 172 tion that is distinct from the present local field. It is likely that these samples acquired
 173 an isothermal remanent magnetization associated with quarrying operations or lightning
 174 strikes. This behavior can be prevalent throughout a site or can be present in just some
 175 samples from a given site. In many cases, these low-coercivity overprints can be removed
 176 through AF demagnetization and the medium-coercivity and/or high-coercivity compo-
 177 nents can be subsequently isolated. In some instances, however, these large and dom-
 178 inantly low-coercivity overprints extend to higher coercivities preventing the isolation
 179 of other components.

180 The medium-coercivity component direction is dominantly removed through ther-
 181 mal demagnetization between 515°C and 565°C consistent with it being held by low-Ti
 182 titanomagnetite. This direction was recovered with site mean direction uncertainty less
 183 than 8 degrees ($\alpha_{95} < 8^\circ$) for 23 sites (Table 1). We interpret this component to be a
 184 primary thermal remanence acquired at the time of dike emplacement as part of the *ca.*
 185 1780 Ma ECMB. This interpretation gains support from the rock magnetic data, an in-
 186 verse baked contact test, and thermochronology data that support an emplacement tem-
 187 perature well below the blocking temperature of magnetite and a mild subsequent ther-
 188 mal history — as discussed in more detail below.

189 **3.1 Magnetic mineralogy constraints from low-temperature magnetom- 190 etry**

191 To gain additional insight into the magnetic mineralogy of the dikes, a Magnetic
 192 Properties Measurement System (MPMS) at the Institute for Rock Magnetism was used
 193 to conduct low-temperature remanence experiments. In the field-cooled (FC) experiments
 194 shown in Figure 4, the magnetization was measured upon warming following the spec-
 195 imen having cooled in an applied field of 2.5 T from 300 to 10 K. In the zero-field-cooled
 196 (ZFC) experiment, a low-temperature saturation isothermal remanence (LTSIRM) of 2.5
 197 T was applied at 10 K after the specimen cooled in a (near-)zero field. In the room-temperature
 198 saturation isothermal remanence (RTSIRM) experiment, the sample was pulsed with a
 199 2.5 T field at room temperature (~ 300 K) and then cooled to 10 K and warmed back
 200 to room temperature in a (near-)zero field. These experiments reveal that sister spec-
 201 imens to paleomagnetic specimens whose remanence is dominated by the medium-coercivity
 202 component without an appreciable high-coercivity component have strong expressions

of the ~120 K Verwey transition as expected for a ferromagnetic mineralogy of well-preserved low-Ti titanomagnetite (NED34-6c in Fig. 4; Verwey (1939); Feinberg et al. (2015)). In contrast, specimens from samples that have a larger contribution of the high-coercivity component have weaker saturation magnetization, minor expression of the Verwey transition, and the presence of monoclinic pyrrhotite as evidenced through the ~30 K Besnus transition (NED36-8c in Fig. 4; Besnus and Meyer (1964); Feinberg et al. (2015)). Samples with a smaller contribution of the high-coercivity component superimposed on the medium-coercivity component have intermediate behavior with a minor expression of the Besnus transition and a more prominent Verwey transition (NED2-8c in Fig. 4). These results support the interpretation that the medium-coercivity component is held by primary unaltered (titano)magnetite and that the high-coercivity component is the result of subsequent alteration that resulted in degradation of magnetite and formation of pyrrhotite.

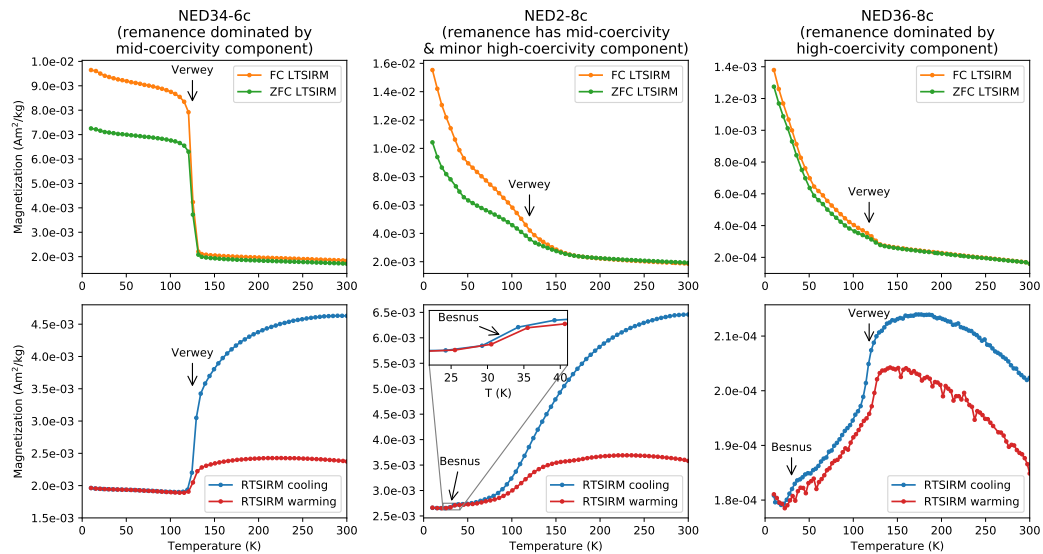


Figure 4. Low-temperature remanence experiment data. The specimen from a sample whose natural remanence is dominated by the medium-coercivity component (NED34-6c) has behavior dominated by magnetite as evidenced through the response across the ~120 K Verwey transition. The specimen from a sample whose natural remanence is dominated by the high-coercivity component (NED36-8c) has weaker magnetization, a relatively minor expression of the Verwey transition, and expression of the ~32 K Besnus transition that indicates the presence of monoclinic pyrrhotite. The specimen whose natural remanence has a well-resolved medium-coercivity component with a minor high-coercivity component (NED2-8c) has intermediate behavior with a Verwey transition that is not as suppressed as in NED36-8c with a minor, but resolvable, Besnus transition (see inset). FC: field-cooled; ZFC: zero-field-cooled; LTSIRM: low-temperature saturation isothermal remanence magnetization; RTSIRM: room-temperature saturation isothermal remanence magnetization.

215 **3.2 Baked contact test**

216 One northwest-trending dike is exposed and was sampled within the study region
 217 as site NWD1 (Fig. 2). The magnetization direction of this dike indicates that it is as-
 218 sociated with the main stage of the Midcontinent Rift (*ca.* 1096 Ma) as it has a normal
 219 polarity and an inclination consistent with that time interval of Midcontinent Rift vol-
 220 canism (Fig. 5; Swanson-Hysell et al. (2020)). The dike cross-cuts one of the northeast-
 221 trending dikes (NED17) allowing for a baked contact test (Figs. 2 and 5). The baked
 222 contact test is positive with a distinct direction in the northeast-trending dike (corre-
 223 sponding to the remanence direction seen throughout the northeast-trending dikes of the
 224 ECMB) with its magnetite remanence becoming progressively overprinted by the northwest-
 225 trending dike up to the contact (Fig. 5). This positive baked contact test indicates that
 226 the northeast-trending ECMB dikes have not been overprinted since the northwest-trending
 227 dike was emplaced (*ca.* 1096 Ma). This positive baked contact test for the northwest-
 228 trending dike constitutes what is referred to as a positive “inverse” baked contact test
 229 for the northeast-trending dike remanence — it constrains the remanence to be more an-
 230 cient than the *ca.* 1.1 Ga Mesoproterozoic northwest-trending dike, but does not pro-
 231 vide a constraint back to the Paleoproterozoic time of dike emplacement. Given that the
 232 host rocks for the northeast-trending dikes are of a very similar age to the dikes them-
 233 selves there is not the possibility of a Paleoproterozoic baked contact test. In contrast
 234 to the dikes, stable and consistent remanence directions were not recovered from pilot
 235 sites in ECMB granites.

236 The high-coercivity remanence direction held by pyrrhotite in some of the northeast-
 237 trending dikes is aligned with the remanence direction of the northwest-trending dike.
 238 While the thermal effect of the northwest-trending dike was limited to a few meters on
 239 either side of it as evidenced through the baked contact test (Fig. 5), there was more
 240 widespread hydrothermal alteration associated with Midcontinent Rift magmatic activ-
 241 ity that led to the formation of pyrrhotite and an associated chemical remanent mag-
 242 netization. In the majority of the northeast-trending dikes, the original magnetite is well-
 243 preserved (e.g., NED34 of Figs. 3 and 4) while other dikes experienced variable magnetite
 244 alteration and the formation of secondary pyrrhotite (e.g., NED36 of Figs. 3 and 4). These
 245 components can be separated through progressive demagnetization (e.g., NED12 of Figs.
 246 3) enabling the thermal remanent magnetization held by magnetite to be used to deter-
 247 mine site mean directions and calculate a paleomagnetic pole (Fig. 6).

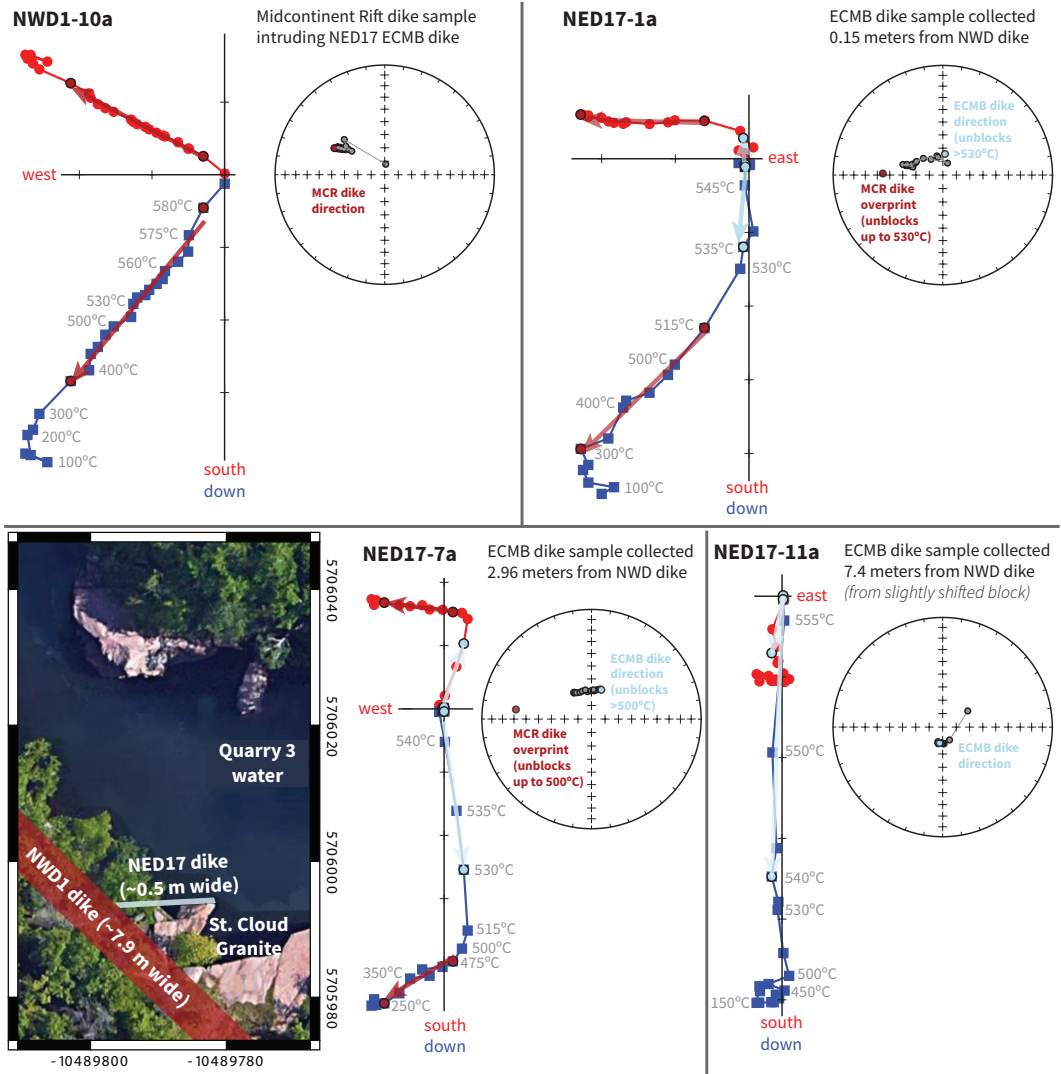


Figure 5. Results from a positive baked contact test where a northwest-trending dike (site NWD1) cross-cuts a northeast-trending dike (site NED17). The NWD1 dike has a direction indicating that it formed during the *ca.* 1096 Ma main stage of rift volcanism. Close to the NWD1 dike the NED17 is nearly fully overprinted (NED17-1a). Further from NWD1 there are partial thermal overprints (NED17-7a) that by ~7 meters from the cross-cutting dike are not resolvable (NED17-11a). Note that blocks from this dike were slightly shifted due to quarrying operations which does not bear on the significance of the positive test, but has led to the exclusion of the result from the site mean compilation and overall pole.

248

3.3 Paleomagnetic pole

249

The site mean directions determined from the magnetite remanence component can be converted to virtual geomagnetic poles and then used to calculate a mean paleomagnetic pole for the ECMB diabase dikes (pole longitude: 265.8°; pole latitude: 20.4°; A₉₅: 4.5°; K: 45.6 N: 23; Fig. 6). These 23 virtual geomagnetic poles have a distribution con-

250

251

252

253 sistent with a Fisher distribution as determined through the Fisher et al. (1987) goodness-
 254 of-fit method. The A₉₅ uncertainty on the mean pole position of 4.5° is within the bounds
 255 of reliability proposed by Deenen et al. (2011). It is well below the A₉₅-max value pro-
 256 posed to establish a well-determined mean for 23 sites (11.4°) and above the A₉₅-min
 257 value (3.4°) consistent with the site directions having sufficiently sampled secular vari-
 258 ation of the geomagnetic field.

259 In a massive host rock such as the ECMB plutons without preferential bedding or
 260 foliation, it is expected that lithospheric stresses will lead to the emplacement of near
 261 vertical dikes. Dike plane orientations were measured on each dike for which there was
 262 sufficient three-dimensional exposure. Multiple measurements were made for each dike
 263 to constrain their orientation. The mean strike calculated from 17 dike orientations is
 264 067° and the mean dip is 88° (Fig. 2). The α_{95} uncertainty associated with the Fisher
 265 mean for the poles to these dike orientation planes (i.e. the lines perpendicular to the
 266 planes) is 4.7° which means that the overall orientation of the planes is statistically in-
 267 distinguishable from vertical (Fig. 2). Due to this verticality, we interpret the exhumation
 268 of the ECMB plutons to have not resulted in appreciable tilting since dike emplace-
 269 ment and do not apply a tilt correction to the paleomagnetic data.

270 4 Geochronology Methods and Results

271 The field relationships show the diabase dikes to be younger than the Rockville Gran-
 272 ite, Reformatory Granodiorite and the St. Cloud Granite which they pervasively intrude
 273 and to be older than the Richmond Granite where they are absent (Boerboom et al., 2005).
 274 Holm et al. (2005) developed U-Pb dates calculated as concordia intercept dates from
 275 these intrusions. The dates reported by Holm et al. (2005) for granites intruded by the
 276 dikes are 1783 ± 11 Ma for the Reformatory Granodiorite, 1780 ± 7 Ma for the Rockville
 277 Granite and 1779 ± 5 Ma for the St. Cloud Granite. The younger cross-cutting Rich-
 278 mond Granite has a date of 1772 ± 3 Ma (Holm et al., 2005). An age of 1774 ± 7 Ma
 279 for one of the quartz-feldspar porphyry dikes developed by Holm et al. (2005) is consis-
 280 tent with this interpretation of these dikes being older than the Richmond Granite (and
 281 younger than the granites they intrude). While the dates published in Holm et al. (2005)
 282 are valuable constraints and are consistent with the field relationships, they are of lower
 283 precision than what is possible with modern analytical approaches and therefore lead
 284 to overlapping uncertainties. Higher precision constraints resulting from methods that

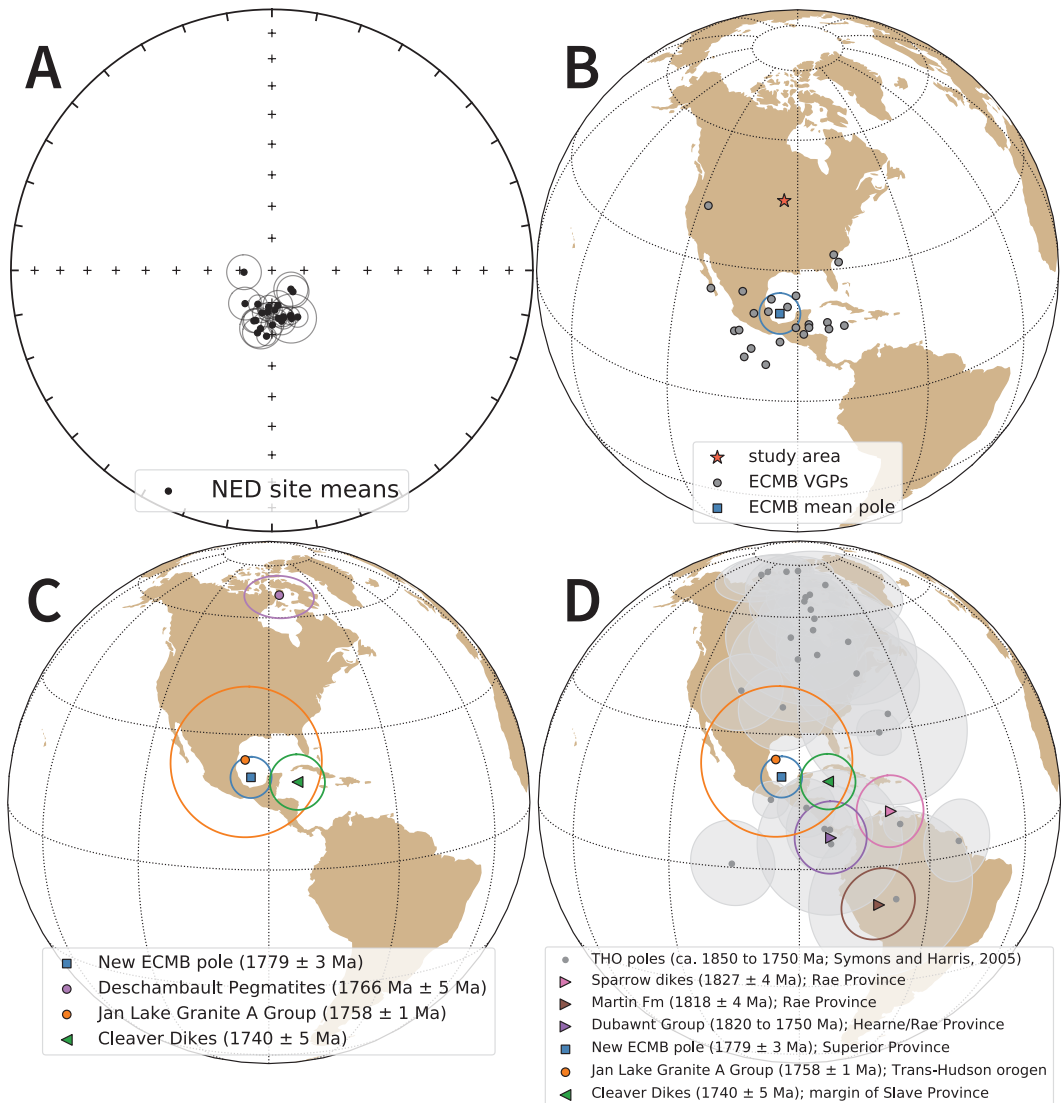


Figure 6. A) Site mean directions for the magnetite remanence of the northeast-trending (NED) ECMB diabase dikes with $\alpha_{95} < 8^\circ$. B) Virtual geomagnetic poles (VGPs) calculated from these site means and the overall mean paleomagnetic pole for the ECMB dikes. C) Comparison between the new ECMB paleomagnetic pole and other ca. 1780 to 1740 Ma poles for Laurentia. D) Comparison of poles from Laurentia's provinces from 1830 to 1740 Ma from Evans et al. (2021) as well as poles from the Trans-Hudson orogen (THO; grey; Symons and Harris (2005)) with the new ECMB pole.

apply ion-exchange separation with low blank analyses of chemically-abraded single zircon grains can test the field relationship interpretations and provide more confidence in the overall age constraints.

To further constrain the age of the northeast-trending diabase dikes, we developed new isotope dilution-thermal ionization mass spectrometry (ID-TIMS) U-Pb zircon dates

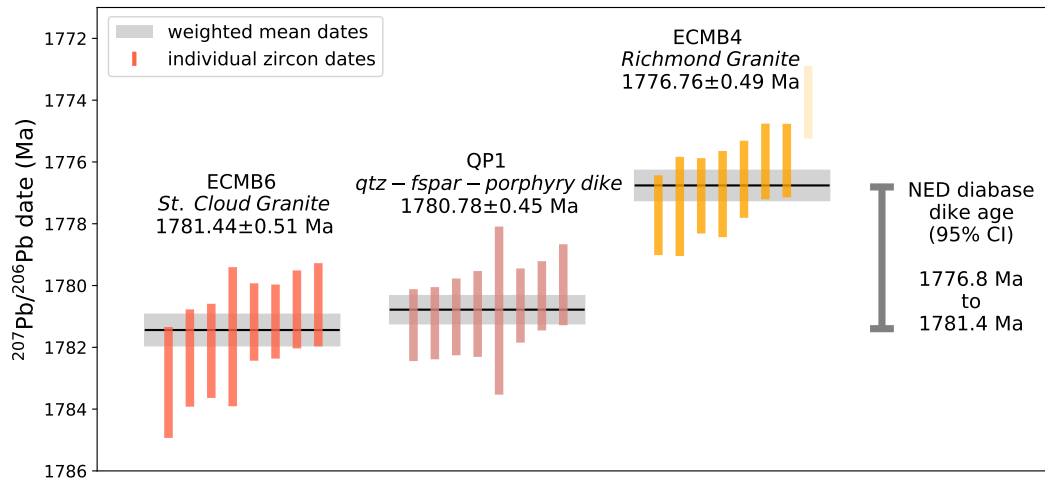


Figure 7. U-Pb dates for ECMB samples. Weighted mean dates (horizontal lines) are calculated from individual zircon dates (vertical bars). The NED diabase dikes intrude the St. Cloud Granite such that the ECMB6 weighted mean date of 1781.44 ± 0.51 Ma is a maximum age. The quartz-feldspar porphyry dikes (one of which was sampled as QP1) also intrude the St. Cloud Granite and are parallel to the NED diabase dikes. Neither the quartz-porphyry dikes nor the diabase dikes intrude the younger cross-cutting Richmond Granite such that the ECMB4 weighted mean date of 1776.76 ± 0.49 Ma provides a minimum age for the dikes. Details for the weighted mean dates are given in Table 2 and individual zircon data are in the Supporting Information.

from the St. Cloud Granite that host the dikes (sample ECMB6), the Richmond Granite from which the dikes are absent (sample ECMB4), and from a northeast-trending quartz-feldspar porphyry dike (sample QP1) that is likely coeval with the diabase dikes (Figs. 2 and 7). Zircon crystals were chemically abraded prior to analysis of single zircon grains by ID-TIMS at the Boise State Isotope Geology Laboratory (detailed geochronology methods are provided in the Supporting Information). Weighted mean dates were calculated from multiple single zircon dates (Fig. 7; Table 2). While chemical abrasion served to reduce Pb-loss and resulted in concordant analyses, some grains have persistent Pb-loss and are discordant (Fig. S1). As a result, we calculate weighted mean $^{207}\text{Pb}/^{206}\text{Pb}$ dates rather than $^{206}\text{Pb}/^{238}\text{U}$ dates (Fig. 7; Table 2). These $^{207}\text{Pb}/^{206}\text{Pb}$ dates are 1781.44 ± 0.51 Ma (2σ analytical uncertainty; MSWD = 1.24; n=8) for the St. Cloud Granite (ECMB6) and 1776.76 ± 0.49 Ma (MSWD = 1.15; n=7) for the Richmond Granite (ECMB4; Fig. 7). The date for the sampled quartz-feldspar porphyry dike (QP1) of 1780.78 ± 0.45 Ma (MSWD = 0.53; n=8) is between these two dates as expected on the basis of field relationships. Taking into account the analytical uncertainty on the maximum and minimum age constraints, the diabase dikes are younger than the 1781.44 ± 0.51 Ma St. Cloud

306 Granite and older than the 1776.76 ± 0.49 Ma Richmond Granite. If one assumes a uni-
 307 form probability of diabase emplacement timing between the maximum and minimum
 308 age constraints that have normally distributed uncertainties, the 95% confidence inter-
 309 val can be estimated through Monte Carlo simulation. Applying this approach gives a
 310 mean age of 1779.1 Ma with 95% confidence interval (CI) bounds of 1776.8 to 1781.4 Ma.
 311 We can succinctly state the age of the northeast-trending ECMB diabase dikes as be-
 312 ing 1779.1 ± 2.3 Ma (95% CI).

313 5 Thermochronology Methods and Results

314 While the U-Pb zircon dates constrain the crystallization ages of the ECMB in-
 315 trusions, additional insight into the thermal history of the batholith can help with in-
 316 terpretation of the paleomagnetic data given that the thermal remanent magnetization
 317 of magnetite will be blocked at temperatures below 580°C. As discussed below, existing
 318 Ar-Ar dates on hornblende and biotite from the ECMB provide valuable constraints in
 319 this regard (Fig. 8). In this study, we also develop new U-Pb apatite dates from three
 320 ECMB granites (ECMB1, the Isle Granite; ECMB3, the Rockville Granite; ECMB4, the
 321 Richmond Granite). In contrast to zircon, for which the temperatures of appreciable Pb
 322 diffusion exceed the liquidus of granite (Cherniak & Watson, 2001), the temperature win-
 323 dow for closure of the U-Pb system in apatite is much lower (~ 510 to 460 °C; Smye et
 324 al. (2018)). As a result, U-Pb dates of apatite serve as a thermochronometer at moderately-
 325 high temperatures (Chamberlain & Bowring, 2001; Schoene & Bowring, 2007; Cochrane
 326 et al., 2014). These temperatures are of particular relevance to the interpretation of the
 327 paleomagnetic data as they are lower than, or correspond with, the blocking tempera-
 328 ture of low-Ti titanomagnetite. If a pluton was emplaced at depths where temperatures
 329 exceed the closure temperature of apatite, or if it experienced prolonged reheating, the
 330 U-Pb apatite dates would be appreciably younger than the U-Pb zircon crystallization
 331 dates.

332 U-Pb data were developed from apatite grains separated from ECMB granites through
 333 laser ablation inductively coupled plasma mass spectrometry (LA-ICP-MS) at UC Santa
 334 Barbara (method details are provided in the supporting information). In contrast to zir-
 335 con, apatite incorporates significant Pb at the time of crystallization. As a result of this
 336 elevated common Pb, U-Pb dates were determined through the calculation of Tera-Wasserburg
 337 concordia lower intercept dates where the upper intercept corresponds to the ratio of ini-

tial $^{207}\text{Pb}/^{206}\text{Pb}$ and the lower intercept is the $^{206}\text{Pb}/^{238}\text{U}$ date (following the method of Ludwig (1998) as implemented in the IsoplotR software of Vermeesch (2018); Fig. S2). Sample ECMB1 is from the Isle Granite which has a U-Pb zircon date of 1779 ± 26 Ma (Holm et al., 2005). The U-Pb apatite date for ECMB1 is $1800.3 \pm 33.4/65.2$ Ma where the first uncertainty is the 2σ analytical uncertainty and the second uncertainty is 95% confidence interval for the date that incorporates overdispersion (this uncertainty scheme will be used for all the presented apatite dates). This U-Pb apatite date is therefore indistinguishable from the U-Pb crystallization date (Fig. 8). Sample ECMB3 is from the Rockville Granite which has a U-Pb zircon date of 1780 ± 7 Ma (Holm et al., 2005). The U-Pb apatite date for ECMB3 is $1810.5 \pm 16.2/23.0$ Ma. The youngest end of the overdispersion uncertainty range is very similar to (albeit just slightly older than) the U-Pb zircon date. It is not geologically reasonable for the U-Pb apatite date to be older than the U-Pb zircon date. This result therefore suggests that the U-Pb apatite date uncertainty is a slight underestimate with the U-Pb apatite system having closed just after the time of zircon crystallization as constrained through the U-Pb zircon date. Sample ECMB4 is from the Richmond Granite for which we have developed a new ID-TIMS U-Pb zircon date of 1776.76 ± 0.49 Ma. The U-Pb apatite date for ECMB4 is $1751.7 \pm 17.8/36.6$ Ma which is indistinguishable from the U-Pb zircon date (Fig. 8).

Pb closure temperatures (T_c) for the analyzed apatite grains can be estimated with the Dodson (1973) approach assuming a cylindrical geometry with half-widths as the characteristic diffusion length. Apatite grain sizes are similar across the three dated specimens; they typically are 100-200 μm long and 50-75 μm wide. Using the Pb diffusivity values of Cherniak et al. (1991), a cooling rate of $20^\circ\text{C}/\text{Myr}$ results in closure temperatures of 463°C to 473°C for these grain sizes. A more rapid cooling rate is likely for the batholith given the similarity of the U-Pb apatite dates with the U-Pb zircon dates. A cooling rate of $100^\circ\text{C}/\text{Myr}$ from crystallization to apatite closure temperatures results in closure temperatures of 493°C to 505°C .

Overall, these data indicate that the samples cooled through the $\sim 500^\circ\text{C}$ closure temperatures of the U-Pb apatite system near the time of zircon crystallization consistent with rapid cooling rates of the plutons (Fig. 8). Additionally, there has not been significant diffusion due to later tectonothermal events. As discussed below, this result is consistent with Ar-Ar hornblende dates from the ECMB granites and supports the magnetite remanence being a primary thermal remanent magnetization.

371 **6 Discussion**

372 **6.1 Thermal history of the ECMB and a primary interpretation of the**
 373 **ECMB dike pole**

374 Prior to the emplacement of the ECMB, Paleoproterozoic host rocks were meta-
 375 morphosed to amphibolite facies during the Penokean orogeny (Holm & Silverstone, 1990).
 376 Emplacement of the ECMB has been hypothesized to be post-orogenic and associated
 377 with an interval of extensional collapse of the orogen (Holm & Lux, 1996; Boerboom &
 378 Holm, 2000). The Al-in-hornblende igneous barometer was applied to the St. Cloud and
 379 Isle Granites of the ECMB by Holm, Darrah, and Lux (1998). This barometer has vary-
 380 ing published calibrations. Applying the pressure calibration of Mutch et al. (2016) to
 381 the data in Holm, Darrah, and Lux (1998) and assuming a 2.7 g/cm^3 overburden gives
 382 an estimated emplacement depth of $10.8 \pm 1.7 \text{ km}$ for the Freedhem Granodiorite, ~ 10.4
 383 $\pm 1.7 \text{ km}$ for the Isle Granite and $13.4 \pm 2.1 \text{ km}$ for the St. Cloud Granite. The cali-
 384 bration of Ague (1997) leads to slightly higher calculated pressures implying depths that
 385 are $\sim 2.3 \text{ km}$ deeper.

386 Thermochronology data give additional insight into emplacement temperatures (and
 387 thereby depth). Both the Ar-Ar hornblende dates published by Holm et al. (2005) and
 388 the U-Pb apatite dates developed in this study from ECMB lithologies are indistinguish-
 389 able from the crystallization ages of the intrusions (Fig. 8). The closure temperature for
 390 Ar in hornblende is ~ 580 to 490°C (Harrison, 1982). The closure of the U-Pb system in
 391 the dated apatite grains is ~ 500 to 460°C . The consistency between the U-Pb zircon crys-
 392 tallization and the U-Pb apatite and Ar-Ar hornblende cooling dates indicates that the
 393 present-day erosion level of the ECMB was at a shallow enough depth that the crustal
 394 temperatures were lower than these closure temperatures at the time of emplacement
 395 of the plutons. Geothermal gradients in continental arc settings are typically between
 396 25 to $45^\circ\text{C}/\text{km}$ – potentially higher at 1.8 Ga (Rothstein & Manning, 2003). Taking a
 397 geothermal gradient of $30^\circ\text{C}/\text{km}$ and the closure temperature constraints indicates that
 398 the plutons were emplaced at 15 km or shallower in the continental lithosphere. This
 399 emplacement depth is consistent with the Al-in-hornblende paleobarometry estimates.

400 Ar-Ar biotite dates provide insight into even lower temperatures as the system blocks
 401 at $\sim 330^\circ\text{C}$ (Grove & Harrison, 1996), well below the blocking temperature of magnetite
 402 magnetization in the dikes. Ar-Ar biotite dates from ECMB plutons range from over-

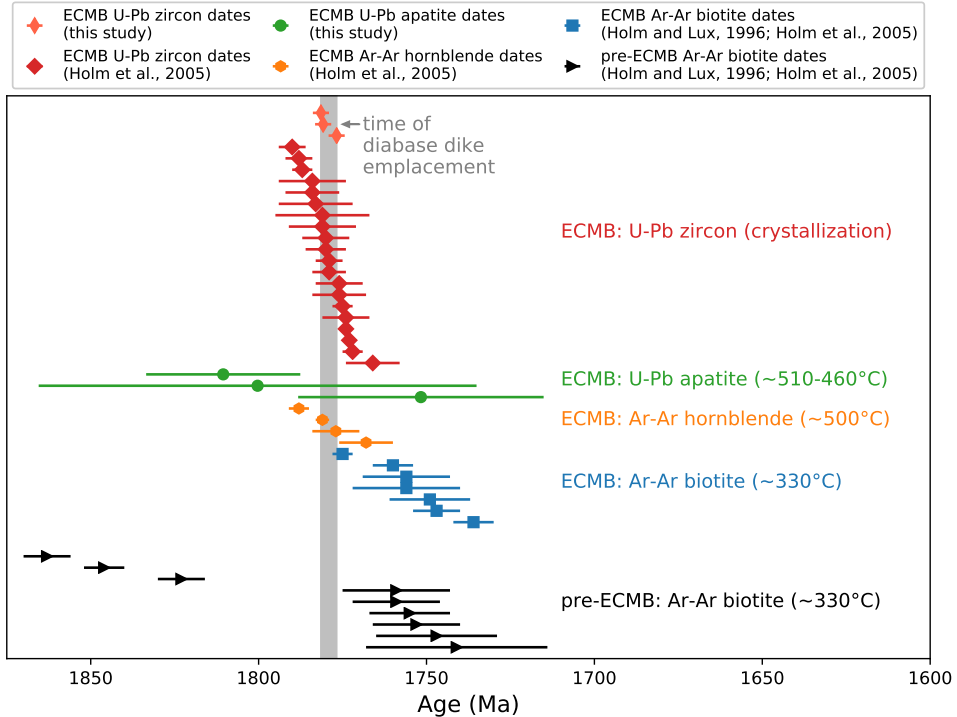


Figure 8. Summary of U-Pb zircon dates, U-Pb apatite dates, Ar-Ar hornblende, and Ar-Ar biotite dates from the East-Central Minnesota batholith (ECMB) from this study, Holm and Lux (1996) and Holm et al. (2005). Approximate closure temperatures associated with the thermochronometers are labeled next to the relevant data. That the U-Pb apatite and Ar-Ar hornblende dates are indistinguishable from the U-Pb zircon crystallization dates indicates that the plutons were emplaced at upper middle to upper crustal levels. The Ar-Ar biotite dates from both the ECMB plutons and older host rock lithologies indicate exhumation within \sim 20 million years to shallower depths and a lack of regional tectonothermal activity over the following 1.75 billion years.

lapping the crystallization dates to being younger by \sim 20 million years (Fig. 8). Ar-Ar biotite dates from older host lithologies to the ECMB are either older than the age of the batholith itself or the same age as the Ar-Ar biotite dates from the batholith (Fig. 8). These data suggest that the batholith was emplaced near the upper depth range estimates from the Al-in-hornblende barometry (\sim 10 km) and underwent exhumation to below the \sim 330°C closure temperature of the K-Ar biotite system soon after emplacement of the plutons. These data also indicate that there has not been reheating or pervasive fluid flow that would have perturbed the Ar-Ar thermochronometers in the granites in the time since initial cooling. The magnetization used to develop the paleomagnetic pole comes from remanence held by low-Ti magnetite that dominantly unblocks between 540 and 560°C (Figs. 3 and 5). The thermochronology results constrain the rocks

414 to have cooled through the magnetite blocking temperatures at the time that the dikes
 415 were emplaced within the batholith and to not have experienced reheating that would
 416 have perturbed the thermochronometers. These data support an interpretation that the
 417 magnetite remanence within the ECMB dikes is a primary thermal remanent magneti-
 418 zation.

419 These thermochronology data also demonstrate that following the emplacement of
 420 the ECMB there were not regional tectonothermal events with the potential to have ther-
 421 mally modified the magnetization of the magnetite within the ECMB diabase dikes. Sub-
 422 sequent Paleoproterozoic Yavapai and Mazatzal accretion occurred to the southeast of
 423 the Spirit Lake Tectonic zone on the other side of the Minnesota River Valley promon-
 424 tory (~160 km south of the study region; Fig. 1; Holm et al. (2007)). In contrast to the
 425 northeast-trending dikes in the ECMB, northeast-trending dikes in Wisconsin within *ca.*
 426 1840 Ma plutons were metamorphosed to amphibolite facies associated with such accre-
 427 tionary orogenesis (Holm et al., 2019). Mazatzal orogeny deformation and metamorphism
 428 occurred *ca.* 1650 to 1630 Ma within the juvenile accreted island arc of the Wisconsin
 429 Magmatic Terrane (Holm, Schneider, & Coath, 1998). The region of the ECMB was not
 430 affected by these tectonothermal events (Fig. 1, Holm et al. (2005)). Holm et al. (2005)
 431 proposed that the voluminous ECMB batholith stabilized the continental lithosphere and
 432 prevented the region from being modified during subsequent collisions along the mar-
 433 gin. This lack of deformation in the region of the ECMB is further supported by the nearly
 434 horizontal bedding of *ca.* 1.63 Ga siliciclastic sedimentary rocks on either side of the batholith
 435 (Holm, Schneider, & Coath, 1998; Medaris et al., 2021). In southwestern Minnesota, plu-
 436 tons coeval with the ECMB are overlain by the subhorizontal Sioux Quartzite (Fig. 1)
 437 with the correlative Barron Quartzite of northwestern Wisconsin also being undeformed
 438 (Southwick et al., 1986). This lack of deformation contrasts with correlative Baraboo
 439 quartzite south of the Spirit Lake Tectonic Zone (~400 km from the ECMB) that un-
 440 derwent compressional deformation during subsequent orogenesis (Holm, Schneider, &
 441 Coath, 1998; Medaris et al., 2021). The Yavapai and Mazatzal terranes were intruded
 442 by *ca.* 1470 to 1430 Ma granites of the Eastern Granite Rhyolite Province and there is
 443 a sizeable pluton of this age within accreted Penokean rocks in northern Wisconsin (the
 444 *ca.* 1470 Ma Wolf River batholith; Dewane and Van Schmus (2007)). However, the ther-
 445 mal effects of the Wolf River batholith (~370 km east of the ECMB study area) were
 446 limited to a 10-15 km wide contact zone surrounding the intrusion (Holm et al., 2019).

The one major subsequent tectonothermal event in the region for which there is localized evidence in the ECMB is the development of the Midcontinent Rift that initiated *ca.* 1109 Ma and in which magmatic activity continued to *ca.* 1084 Ma (Fig. 1; Fairchild et al. (2017); Swanson-Hysell et al. (2019)). While the main rift axis can be inferred from gravity and aeromagnetic anomaly data to be located \sim 75 km southeast of the study region (Fig. 1), the studied northwest-trending dike has a magnetization direction that implies that it was emplaced during Midcontinent Rift development *ca.* 1096 Ma (Fig. 5). The baked contact test between that dike (NWD1) and the northeast-trending dike that it cross-cuts (NED17), indicates that the thermal effect of the dike emplacement and the Midcontinent Rift in general was localized within the immediate vicinity of that dike (a few meters; Fig. 5). However, this Midcontinent Rift magmatic activity did result in local hydrothermal alteration as evidenced by magnetization held by monoclinic pyrrhotite that is variably present through the ECMB dikes and is in the same direction as the magnetization of the northwest-trending dike (Fig. 3). This chemical remanent magnetization held by monoclinic pyrrhotite likely formed at relatively low temperatures. Phase relationships in the Fe-S system developed through hydrothermal recrystallization experiments show monoclinic pyrrhotite to form at temperatures below 250°C and likely above 75°C (Kissin & Scott, 1982). While in some sites, this pyrrhotite-forming alteration obscured the primary thermal remanence held by magnetite (e.g., NED36 in Fig. 3), in the majority of sites the magnetite remanence direction can be well-resolved (e.g., NED2, NED12 and NED34 in Fig. 3). As a result, the paleomagnetic directions used to calculate the paleomagnetic pole shown in Figure 6 are held by (titano)magnetite that recorded a thermal remanent magnetization upon cooling of the diabase dikes. This evidence for variable late Mesoproterozoic hydrothermal alteration of the dikes provides an explanation for Ar-Ar data developed from two northeast-trending diabase dikes that were reported in Boerboom and Holm (2000). These Ar-Ar data did not yield a plateau age, but give whole rock total gas dates that are late Mesoproterozoic in age. An interpretation that these whole rock total gas ages correspond with the age of emplacement is difficult to reconcile with the cogenetic relationship between the diabase dikes, the quartz-feldspar porphyry dikes and the ECMB granites. K-Ar whole-rock ages of 1570 to 1280 Ma from the dikes reported in Hanson (1968) and discussed in Horan et al. (1987) are attributed to partial resetting. The evidence for fluid flow that led to the formation of pyrrhotite *ca.* 1096 Ma supports the hypothesis put forward by Horan et al. (1987), as

480 well as by Boerboom and Holm (2000), that there was Mesoproterozoic disruption of the
 481 K-Ar isotopic system in the dikes such that the Mesoproterozoic Ar-Ar dates are the re-
 482 sult of alteration of dikes which are Paleoproterozoic in age. The field relationships in-
 483 dicating that the northeast-trending diabase dikes are comagmatic with ECMB gran-
 484 ites is also consistent with whole rock Pb isotope data that reveal very similar arrays im-
 485 plying a *ca.* 1.8 Ga isochron age for both lithologies (Horan et al., 1987).

486 Overall, the constraints requiring that the ECMB granites were emplaced at depths
 487 where the ambient temperature was below the closure of U-Pb apatite and Ar-Ar horn-
 488 blende systems indicate that the comagmatic diabase dikes would have acquired their
 489 magnetization at the time of emplacement. The lack of significant thermal events that
 490 could have reset the magnetite magnetization is indicated by the geologic setting, the
 491 thermochronology data (including the Paleoproterozoic Ar-Ar biotite dates), and the pos-
 492 itive inverse baked contact test. We therefore interpret the pole calculated from the mag-
 493 netite remanence of the ECMB diabase dikes as a high-quality constraint on the pale-
 494 ogeographic position of Laurentia at the time the dikes intruded (1779.1 ± 2.3 Ma). The
 495 ECMB diabase dikes pole meets six of the seven criteria for the quality criteria Van der
 496 Voo (1990) and the Meert et al. (2020) reliability criteria with the only one not satis-
 497 fied being due to the lack of dual polarity directions. This single polarity normal polar-
 498 ity is consistent with the polarity of the Cleaver Dykes and the proposal of Irving (2004)
 499 that there was a normal geomagnetic superchron that followed the Trans-Hudson orogeny.

500 6.2 Laurentia's paleomagnetic poles following the Trans-Hudson orogeny

501 The Trans-Hudson orogeny is a major event in the formation of Laurentia result-
 502 ing from collision between the Superior province and the Churchill plate consisting of
 503 the composite Slave + Rae + Hearne provinces (Hoffman, 1988; Corrigan et al., 2009;
 504 Weller & St-Onge, 2017). Geologic data on the timing of Trans-Hudson orogenesis in-
 505 clude a $^{206}\text{Pb}/^{238}\text{U}$ date of 1854.2 ± 1.6 Ma from the base of a foredeep sedimentary suc-
 506 cession on the northern margin of the East Superior province that constrains flexural sub-
 507 sidence associated with Trans-Hudson orogenesis to have initiated at that time (Hodgskiss
 508 et al., 2019). This timing of orogenesis is consistent with $^{207}\text{Pb}/^{206}\text{Pb}$ dates of monazite
 509 within garnet of Trans-Hudson orogen eclogites for which a mean date of 1831 ± 5 Ma
 510 has been interpreted to record peak metamorphism (Weller & St-Onge, 2017). A sim-
 511 ilar timing of *ca.* 1860 to 1820 Ma peak Trans-Hudson metamorphism resulting from col-

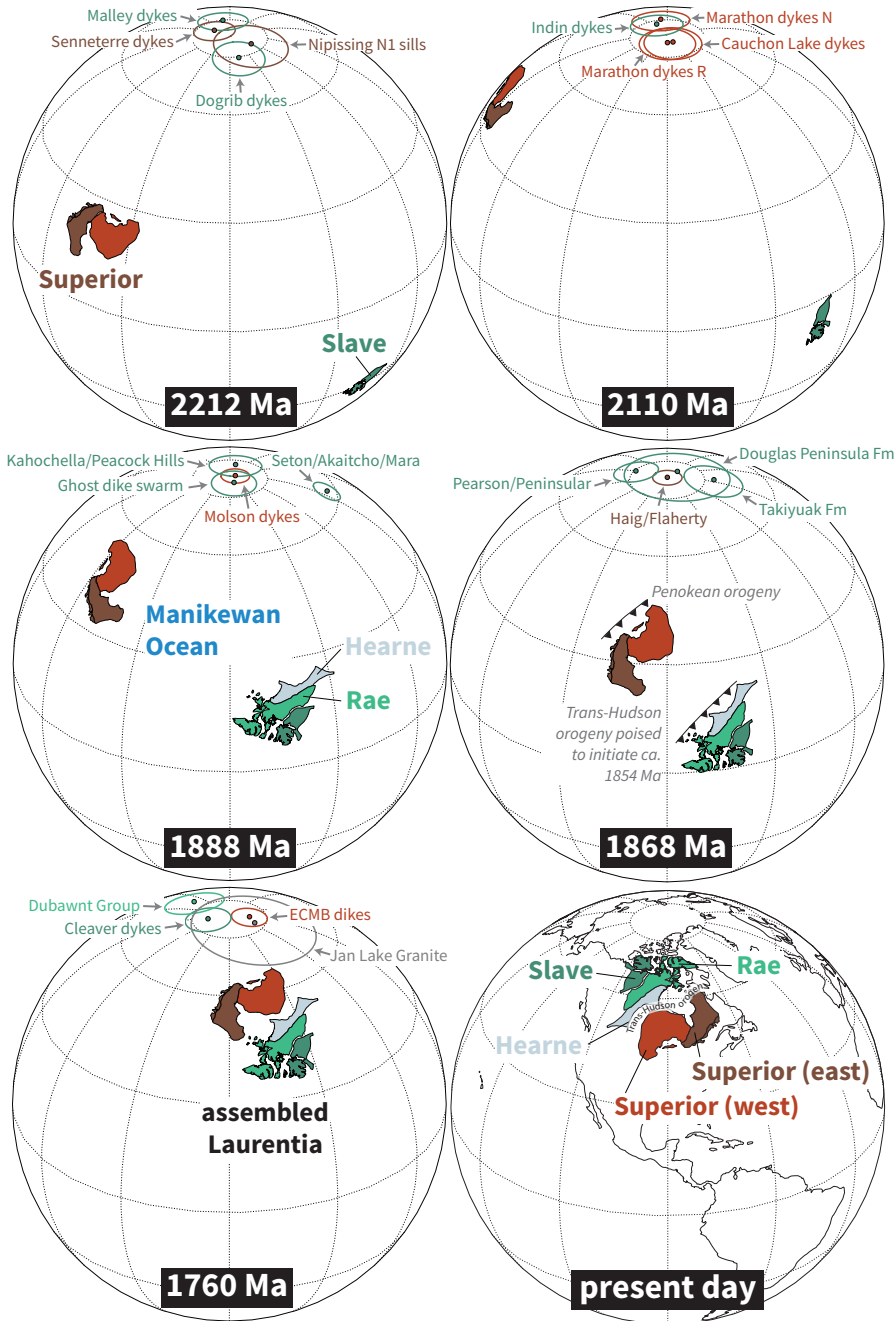


Figure 9. Paleogeographic reconstructions at five different times in the Paleoproterozoic and the position of the provinces at present. Paleomagnetic poles within 20 Myr of the given time (10 Myr for 1888 and 1868 Ma) are shown from the compilation of Evans et al. (2021) as well as the new ECMB pole. These data illustrate differential plate motion between the Superior and Slave Provinces that is required by the data leading up to the closure of the Manikewan Ocean and the assembly of Laurentia during the Trans-Hudson orogeny. The ECMB pole is consistent with an assembled Laurentia following the Trans-Hudson orogeny which contrasts with the disparate orientations and paleolatitudes between Laurentia's constituent provinces prior to the orogeny.

512 lisional orogenesis has been interpreted from U-Pb zircon rim and monazite dates from
 513 the orogen in Baffin Island, Nunavut, Canada (Skipton et al., 2016). These geologic data
 514 strongly support that the Superior Province was conjoined with the Slave + Rae + Hearne
 515 provinces prior to 1800 Ma in their present-day relative positions (Fig. 1). There are high-
 516 quality paleomagnetic poles for the Superior province during the time interval when the
 517 Manikewan Ocean was closing leading up to the Trans-Hudson orogeny (the *ca.* 1880 Mol-
 518 son dykes pole and the *ca.* 1870 Ma Haig/Flaherty pole; Fig. 9). There are no Paleo-
 519 proterozoic paleomagnetic poles for the Superior Province during or after the Trans-Hudson
 520 orogeny that can test Laurentia's coherency with paleomagnetic data. The new 1779.1 ± 2.3 Ma ECMB
 521 paleomagnetic pole fills this gap.

522 While abundant paleomagnetic data have been developed from rocks within the
 523 Trans-Hudson orogen (Symons & Harris, 2005), both the primary nature of the rema-
 524 nance directions as well as the age of remanence acquisition has been challenging to es-
 525 tablish. As a result, relatively few poles from this interval during and following Lauren-
 526 tia's amalgamation have been included in curated pole compilations such as that com-
 527 piled by the Nordic paleogeography workshops (Evans et al., 2021). The best constrained
 528 of these poles comes from the post-orogenic 1740 ± 5 Ma Cleaver Dykes of the Great
 529 Bear Magmatic Arc on the western margin of the Slave Province (Fig. 1; Irving (2004)).
 530 The age of these dikes is constrained by a U-Pb baddeleyite date and there is a positive
 531 baked contact test supporting the interpretation that the pole is primary. As can be seen
 532 in Figure 6, the position of this *ca.* 1740 Ma Cleaver Dykes pole for Laurentia (Irving,
 533 2004) is similar to the new pole for the *ca.* 1780 Ma ECMB diabase dikes (Fig. 6). They
 534 do not share a common mean (as determined through Watson and bootstrap common
 535 mean tests; Tauxe et al. (2016)), but are within 11° of one another (less when consid-
 536 ering uncertainty). The similarity in these pole positions provides an independent test
 537 of the coherency of the Laurentia craton at that time.

538 An additional pole for comparison comes from hematite remanence of volcanics and
 539 sediments of the Baker Lake Group of the Dubawnt Supergroup which were deposited
 540 in a basin atop the suture between the Rae and Hearne provinces (Figs. 1 and 6; Park
 541 et al. (1973)). Both the depositional age of the succession and the age of hematite re-
 542 manence are roughly constrained leading to a wide assigned age range of 1820 to 1750
 543 Ma in Evans et al. (2021) for the pole. While the loose age constraints hinder firm com-
 544 parisons, the broad similarity of this pole with the Cleaver Dykes pole of the Slave Province

545 as well as that for Martin Formation (1818 ± 4 Ma) and the Sparrow dikes (1827 ± 4
 546 Ma) of the Rae Province establishes a largely consistent position of the Churchill plate
 547 from *ca.* 1820 to 1740 Ma.

548 A less robust pole for comparison with the new ECMB pole comes from the post-
 549 orogenic Jan Lake Granite within the Trans-Hudson orogen in southeast Saskatchewan
 550 developed in Gala et al. (1995). A U-Pb zircon date of 1758 ± 1 Ma for this granite was
 551 reported in Bickford et al. (2005). Directional data from the Jan Lake Granite falls into
 552 two groups. Based on thermal demagnetization behavior, Irving (2004) interpreted the
 553 ‘A’ grouping to be a TRM held by magnetite that was acquired at the time of the em-
 554 placement of the intrusion *ca.* 1758 Ma. The ECMB dikes pole shares a common mean
 555 with this Jan Lake Granite pole with overlapping A₉₅ confidence circles (Fig. 6). This
 556 result is consistent with both the Jan Lake Granite and ECMB being post-orogenic mag-
 557 matic events that occurred following the amalgamation of Laurentia. This similarity sug-
 558 gests that despite the large uncertainty on the Jan Lake Granite pole and the ambigu-
 559 ity resulting from multiple directional groups that the pole does constrain the position
 560 of Laurentia *ca.* 1758 Ma.

561 A pole that does not hold up to such comparative scrutiny is that developed for
 562 the Deschambault Pegmatites from within the Trans-Hudson orogen (Fig. 6C; Symons
 563 et al. (2000)). This pole has been interpreted to constrain the position of Laurentia *ca.*
 564 1766 Ma — an age based on U-Pb monazite and allanite dates of other pegmatites in
 565 the region. As noted in D’Agrella-Filho et al. (2020), there are no field tests for this pole
 566 and the remanence directions from which it is calculated are quite close to the modern
 567 geomagnetic field. This pole was included in the curated Nordic paleogeography work-
 568 shop compilation of Evans et al. (2021) less because of the quality of the individual pole,
 569 but rather because there are a number poles of similar position to this one from the Trans-
 570 Hudson orogen (Fig. 6). Many of these poles have individual VGPs that are streaked
 571 between directions similar to the Jan Lake Granite and that of the present-local field.
 572 The direction of the Deschambault pole is far from the new *ca.* 1780 Ma ECMB dikes
 573 pole. In contrast, the similarity of pole position between the new ECMB dikes pole and
 574 the *ca.* 1758 Ma Jan Lake Granite pole as well as the *ca.* 1740 Ma Cleaver Dykes pole
 575 supports that these poles, rather than the Deschambault Pegmatites pole, constrain Lau-
 576 rentia’s position during this interval. This Deschambault Pegmatites pole played a role,
 577 in conjunction with other poles from the Trans-Hudson orogen, such as that from the

578 Wapisu gneiss and the Deschambault Post pluton, in an interpretation that Laurentia's
 579 pole path was at a standstill in the vicinity of the Deschambault Pegmatites pole from
 580 *ca.* 1800 Ma through to *ca.* 1766 Ma (Symons et al., 2000; Symons & Harris, 2005). As
 581 reviewed in Raub (2008), there are numerous difficulties in interpreting these data from
 582 the Trans-Hudson orogen as useful constraints including: 1) a lack of field tests; 2) un-
 583 certainty in the timescale of cooling and the timing of the acquisition of magnetization
 584 in these slowly cooled units; 3) poorly constrained tilt corrections and 4) large secondary
 585 viscous remanent magnetizations that are prevalent due to the coarse grain-size of the
 586 igneous lithologies. The preferred interpretation of Raub (2008), which is echoed in D'Agrella-
 587 Filho et al. (2020), is that there is unresolved component mixing between primary di-
 588 rections (which would be in the vicinity of the Jan Lake Granite A Group pole and our
 589 new ECMB pole) and the present-day north pole as the result of unresolved viscous over-
 590 prints (Fig. 6). This component mixing leads to streaked site mean directions in indi-
 591 vidual studies as well as the database of Trans-Hudson orogen poles including the De-
 592 schambault Pegmatites pole (Fig. 6; Raub (2008)). The new ECMB pole significantly
 593 strengthens this interpretation by demonstrating that a proposed northerly apparent po-
 594 lar wander path to satisfy the Deschambault Pegmatites pole and other Trans-Hudson
 595 orogen poles streaked between the Jan Lake Granite and the modern-day pole is indeed
 596 fictitious (Fig. 6). Instead, the ECMB pole and the Cleaver Dykes pole establish the pa-
 597 leogeographic position of Laurentia to have been consistent *ca.* 1780 to 1740 Ma (Fig.
 598 9).

599 6.3 The paleogeography of Laurentia

600 As is expected by the geologic record of Trans-Hudson orogenesis, the similarity
 601 in pole positions from the southeastern margin of the Superior Provinces (the new ECMB
 602 pole) and the northwestern margin of the Slave Province (the Cleaver Dykes pole; Fig.
 603 6) indicate a coherent assembled Laurentia following 1.8 Ga (Fig. 9). The coherency of
 604 the record of high-quality paleomagnetic poles at this time when the geologic record in-
 605 dicates a recently assembled Laurentia increases confidence that differing pole positions
 606 between Laurentia's Archean provinces earlier in the Paleoproterozoic are indeed a record
 607 of differential plate tectonic motion (Fig. 9). There is a particularly rich record of pa-
 608 leomagnetic poles from the Archean Superior and Slave provinces that can be paired be-
 609 tween 2.23 and 1.89 Ga that constrain the provinces to not be in their modern relative

610 orientation and to be undergoing differential motion (Mitchell et al., 2014; Buchan et
611 al., 2016; Swanson-Hysell, 2021). These poles result in reconstructions where prior to the
612 Trans-Hudson orogeny there was an ocean basin between the Superior province and the
613 Hearne + Rae + Slave provinces known as the Manikewan Ocean (Fig. 9; Stauffer (1984)).
614 The poles are consistent with the Superior Province approaching the joint Slave + Hearne
615 + Rae provinces prior to the onset of the Trans-Hudson orogeny (Fig. 9). These data
616 provide strong evidence for mobile lid plate tectonics from 2.23 Ga onward (Mitchell et
617 al., 2014; Buchan et al., 2016; Swanson-Hysell, 2021).

618 The orogenesis associated with Laurentia's assembly is hypothesized to have re-
619 sulted in the formation of the supercontinent, or semi-supercontinent, Nuna (Hoffman,
620 1997; Evans & Mitchell, 2011; Evans et al., 2016). Given that Laurentia is the largest
621 craton hypothesized to have been part of this supercontinent, its paleogeographic po-
622 sition is key to reconstructions of Nuna. The new ECMB pole provides higher confidence
623 in the paleogeographic position of Laurentia in the time just following its formation from
624 the collision of constituent Archean provinces (Fig. 9). This new pole can be used to eval-
625 uate hypothesized connections between Laurentia and other cratons. There is an increas-
626 ingly rich global database of paleomagnetic poles *ca.* 1780 Ma including poles from the
627 Amazonia, Baltica, India, Rio de la Plata, São Francisco and North China cratons (Zhang
628 et al., 2012; Xu et al., 2014; Bispo-Santos et al., 2014; Shankar et al., 2018; D'Agrella-
629 Filho et al., 2020).

630 One hypothesized connection of particular interest is that with Baltica. The two
631 cratons have been hypothesized to have been conjoined such that they shared a margin
632 with a long-lived history of accretionary orogenesis (Hoffman, 1997; Karlstrom et al., 2001).
633 The proposed NENA (northern Europe and North America) configuration between Lau-
634 rentia and Baltica allows for such a shared margin (Gower et al., 1990; Buchan et al.,
635 2000; Evans & Pisarevsky, 2008). The increased concordance between *ca.* 1780 to 1750
636 paleomagnetic poles from Laurentia and Baltica upon the NENA rotation of Baltica can
637 be seen in Figure 10. Paleomagnetic poles support a continued NENA connection un-
638 til at least 1260 Ma (supported by poles from Baltica's *ca.* 1258 Ma post-Jotnian intru-
639 sions and Laurentia's *ca.* 1267 Ma Mackenzie dikes) and perhaps to 1120 Ma (where the
640 paleomagnetic comparison is reliant on the *ca.* 1122 Ma Salla dike of Baltica developed
641 from a single cooling unit; Salminen et al. (2009)). This connection supports the long-
642 lived active margin where Laurentia grew through the rest of the Paleoproterozoic and

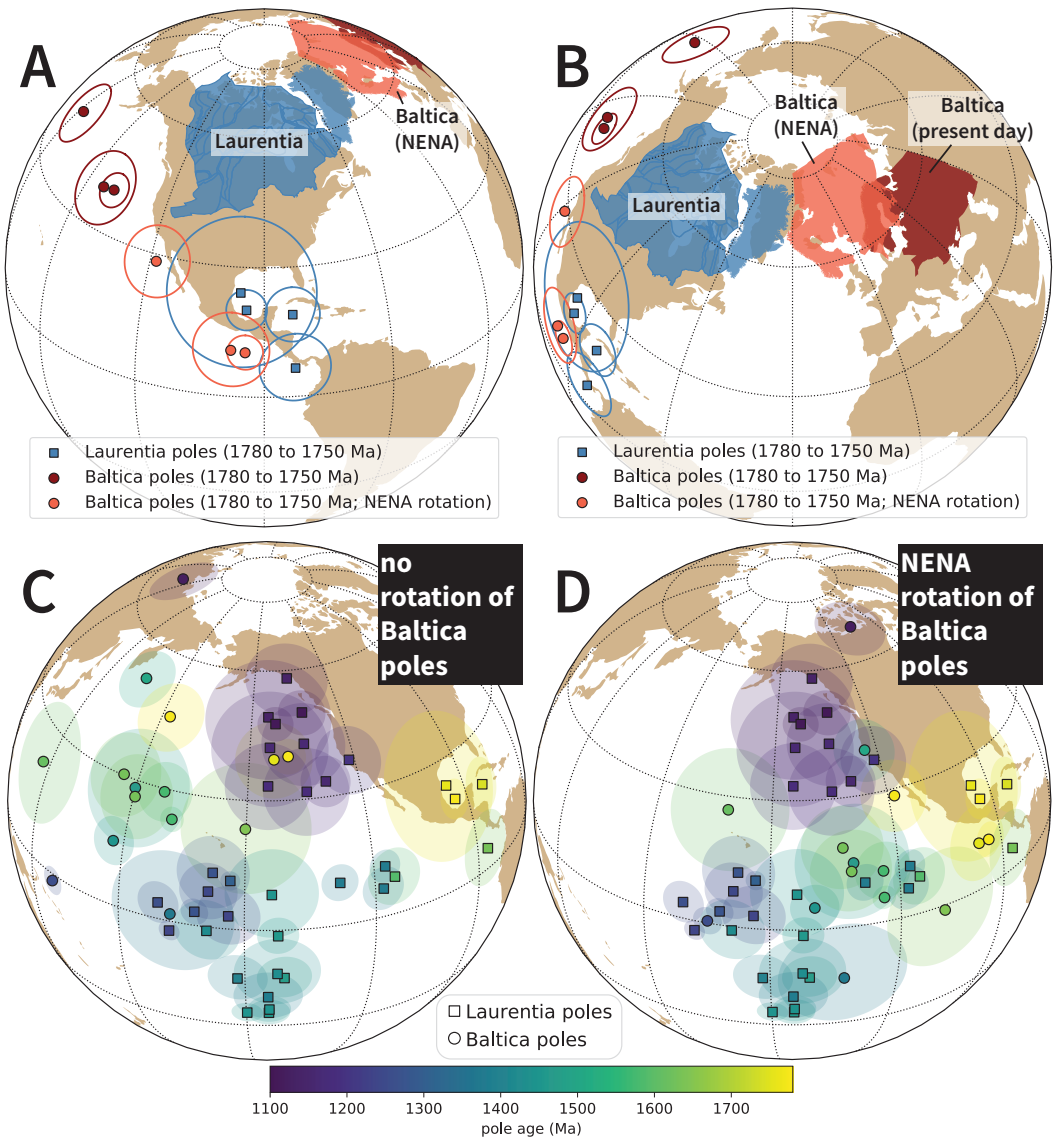


Figure 10. A) Paleomagnetic poles for Laurentia and Baltica between 1780 and 1750 Ma with the Baltica poles shown with and without the NENA rotation (Euler pole for Baltica of $[47.5^\circ, 001.5^\circ, +49.0^\circ]$ as in Evans and Pisarevsky (2008)). Baltica is shown in its present day location in dark red and shown in the NENA position in light red. B) Same data as in panel A shown with a different center of projection which allows for easier visualization of the reconstructed position. C,D) Comparison between poles between 1780 and 1110 Ma between Baltica and Laurentia without (C) and with (D) the NENA rotation. The poles that are shown are those from the Nordic compilation with 'A' and 'B' grades as well as the new ECMB pole from this study.

through the Mesoproterozoic until the *ca.* 1.08 Ga continent-continent collision of the Grenvillian orogeny (Whitmeyer & Karlstrom, 2007).

645 **7 Conclusions**

The East-Central Minnesota Batholith was emplaced following Penokean orogenesis on the southeast margin of the Superior Province. While the southeast margin of Laurentia experienced subsequent intervals of accretionary orogenesis, thermochronology data constrain the batholith to have a straight-forward history of post-emplacement rapid exhumation without substantial reheating. Subsequent orogenesis occurred well southeast of the batholith — consistent with the batholith having played a role in stabilizing Laurentian lithosphere. Comagmatic diabase dikes of the East-Central Minnesota Batholith can be constrained through U-Pb geochronology on the felsic units to have been emplaced at 1779.1 ± 2.3 Ma. A new paleomagnetic pole developed from the magnetite remanence of these dikes provides a high-quality constraint on the position of Laurentia following Trans-Hudson orogenesis. This pole confirms the coherency of an amalgamated Laurentia at the time and supports the NENA connection with Baltica. This paleomagnetic coherency further strengthens the case that previously disparate pole positions between the Superior and Slave provinces are the result of *ca.* 2.2 to 1.8 Ga mobile-lid plate tectonics. The geologic and paleomagnetic record of Laurentia is inconsistent with a stagnant-lid regime anytime over the past 2.2 billion years.

662 **Acknowledgments**

This research was supported by the National Science Foundation through CAREER grant EAR-1847277 awarded to N.L.S.-H.. Rock magnetic experiments using the MPMS were conducted at the Institute for Rock Magnetism which is supported by the Instrumentation and Facilities program of the National Science Foundation, Earth Science Division. We gratefully acknowledge Mark Schmitz and Jim Crowley for analytical support at the Boise State Isotope Geology Laboratory. Noah McLean provided insight for the methodology applied to interpret the uncertainty associated with the age of a unit bracketed by U-Pb dates. We thank Stearns County Parks for research permits that enabled sample collection in Quarry Park and Nature Preserve. The manuscript was improved through thoughtful reviews from Daniel Holm, Anthony Pivarunas, and an anonymous reviewer. Paleomagnetic data associated with this study are available within the MagIC database (<https://earthref.org/MagIC/17072/162b766f-435a-4053-bf63-0a5246c24339>; UPDATE TO DOI WHEN ASSIGNED) and all data are within a Github repository associated with this work (https://github.com/Swanson-Hysell-Group/2021_ECMB) that

677 is also archived on Zenodo (<https://doi.org/10.5281/zenodo.4625041>). This repository
 678 also contains Python code related to calculations, visualizations and statistical tests dis-
 679 cussed herein.

680 **References**

- 681 Ague, J. J. (1997). Thermodynamic calculation of emplacement pressures for
 682 batholithic rocks, California: Implications for the aluminum-in-hornblende
 683 barometer. *Geology*, 25(6), 563. doi: 10.1130/0091-7613(1997)025<0563:
 684 tcoepf>2.3.co;2
- 685 Besnus, M. J., & Meyer, A. J. (1964). Nouvelles données expérimentales sur le
 686 magnétisme de la pyrrhotine naturelle. In *Proc. int. conf. mag.* (Vol. 20,
 687 p. 507-511).
- 688 Bickford, M. E., Mock, T. D., Steinhart III, W. E., Collerson, K. D., & Lewry, J. F.
 689 (2005). Origin of the Archean Sask craton and its extent within the Trans-
 690 Hudson orogen: evidence from Pb and Nd isotopic compositions of basement
 691 rocks and post-orogenic intrusions. *Canadian Journal of Earth Sciences*, 42,
 692 659–684. doi: 10.1139/e04-064
- 693 Bispo-Santos, F., D’Agrella-Filho, M. S., Trindade, R. I., Janikian, L., & Reis, N. J.
 694 (2014). Was there SAMBA in Columbia? Paleomagnetic evidence from 1790
 695 Ma Avanavero mafic sills (northern Amazonian Craton). *Precambrian Re-*
 696 *search*, 244, 139–155. doi: 10.1016/j.precamres.2013.11.002
- 697 Boerboom, T. J., & Holm, D. K. (2000). Paleoproterozoic Intrusive Igneous Rocks of
 698 Southeastern Stearns County, Central Minnesota. *Minnesota Geological Survey*
 699 *Report of Investigations* 56.
- 700 Boerboom, T. J., Holm, D. K., & Van Schmus, R. (2011). Late Paleoproterozoic
 701 deformational, metamorphic, and magmatic history of east-central Minnesota.
 702 *Archean to Anthropocene: Field Guides to the Geology of the Mid-Continent of*
 703 *North America*, 1–23. doi: 10.1130/2011.0024(01)
- 704 Boerboom, T. J., Holm, D. K., & Van Schmus, W. R. (2005). Granites of the East-
 705 Central Minnesota Batholith. *Minnesota Geological Survey Guidebook*.
- 706 Boerboom, T. J., Setterholm, D. R., & Chandler, V. W. (1995). Bedrock geology pl.
 707 2. In G. N. Meyer (Ed.), *Geologic atlas of Stearns County, Minnesota: Min-*
 708 *nesota Geological Survey County Atlas C-10, pt. A., 7 pls., scales 1:100,000*

- 709 and 1:200,000. Minnesota Geological Survey.
- 710 Buchan, K. L., Mertanen, S., Park, R., Pesonen, L., Elming, S. A., Abrahamsen, N.,
 711 & Bylund, G. (2000). Comparing the drift of Laurentia and Baltica in the
 712 Proterozoic: the importance of key paleomagnetic poles. *Tectonophysics*, 319,
 713 167-198. doi: 10.1016/S0040-1951(00)00032-9
- 714 Buchan, K. L., Mitchell, R. N., Bleeker, W., Hamilton, M. A., & LeCheminant,
 715 A. N. (2016). Paleomagnetism of ca. 2.13–2.11 Ga Indin and ca. 1.885
 716 Ga Ghost dyke swarms of the Slave craton: Implications for the Slave
 717 craton APW path and relative drift of Slave, Superior and Siberian cra-
 718 tons in the Paleoproterozoic. *Precambrian Research*, 275, 151–175. doi:
 719 10.1016/j.precamres.2016.01.012
- 720 Chamberlain, K. R., & Bowring, S. A. (2001). Apatite–feldspar U–Pb ther-
 721 mochrochronometer: a reliable, mid-range (\sim 450°C), diffusion-controlled system.
 722 *Chemical Geology*, 172(1-2), 173–200. doi: 10.1016/s0009-2541(00)00242-4
- 723 Cherniak, D., Lanford, W., & Ryerson, F. (1991). Lead diffusion in apatite
 724 and zircon using ion implantation and Rutherford backscattering tech-
 725 niques. *Geochimica et Cosmochimica Acta*, 55(6), 1663–1673. doi:
 726 10.1016/0016-7037(91)90137-t
- 727 Cherniak, D., & Watson, E. (2001). Pb diffusion in zircon. *Chemical Geology*, 172(1-
 728 2), 5–24. doi: 10.1016/s0009-2541(00)00233-3
- 729 Cochrane, R., Spikings, R. A., Chew, D., Wotzlaw, J.-F., Chiaradia, M., Tyrrell, S.,
 730 ... der Lelij, R. V. (2014). High temperature (>350°C) thermochronology and
 731 mechanisms of Pb loss in apatite. *Geochimica et Cosmochimica Acta*, 127,
 732 39–56. doi: 10.1016/j.gca.2013.11.028
- 733 Corrigan, D., Pehrsson, S., Wodicka, N., & de Kemp, E. (2009). The Palaeoprotero-
 734 zoic Trans-Hudson Orogen: a prototype of modern accretionary processes. *Ge-
 735 ological Society, London, Special Publications*, 327(1), 457–479. doi: 10.1144/
 736 sp327.19
- 737 D'Agrella-Filho, M. S., Teixeira, W., da Trindade, R. I., Patroni, O. A., & Prieto,
 738 R. F. (2020). Paleomagnetism of 1.79 Ga Pará de Minas mafic dykes: Testing
 739 a São Francisco/Congo-North China-Rio de la Plata connection in Columbia.
Precambrian Research, 338, 105584. doi: 10.1016/j.precamres.2019.105584
- 740 Deenen, M. H. L., Langereis, C. G., van Hinsbergen, D. J. J., & Biggin, A. J.

- 742 (2011). Geomagnetic secular variation and the statistics of palaeomag-
743 netic directions. *Geophysical Journal International*. doi: 10.1111/
744 j.1365-246X.2011.05050.x
- 745 Dewane, T., & Van Schmus, W. (2007). U-Pb geochronology of the Wolf River
746 batholith, north-central Wisconsin: Evidence for successive magmatism be-
747 tween 1484 Ma and 1468 Ma. *Precambrian Research*, 157(1-4), 215–234. doi:
748 10.1016/j.precamres.2007.02.018
- 749 Dodson, M. H. (1973). Closure temperature in cooling geochronological and petro-
750 logical systems. *Contributions to Mineralogy and Petrology*, 40(3), 259–274.
751 doi: 10.1007/bf00373790
- 752 Evans, D. A. D., Li, Z. X., & Murphy, J. B. (2016). Four-dimensional context of
753 Earth's supercontinents. In D. A. D. Evans, Z. X. Li, & J. B. Murphy (Eds.),
754 *Supercontinent cycles through earth history* (Vol. 424). Geological Society, Lon-
755 don, Special Publications. doi: 10.1144/SP424.12
- 756 Evans, D. A. D., & Mitchell, R. N. (2011). Assembly and breakup of the core of
757 Paleoproterozoic–Mesoproterozoic supercontinent Nuna. *Geology*, 39, 443–446.
758 doi: 10.1130/G31654.1
- 759 Evans, D. A. D., Pesonen, L. J., Eglington, B. M., Elming, S.-Å., Gong, Z., Li, Z.-
760 X., ... Zhang, S. (2021). An expanding list of reliable paleomagnetic poles
761 for Precambrian tectonic reconstructions. In L. J. Pesonen, D. A. D. Evans,
762 S. Å. Elming, J. M. Salminen, & T. Veikkolainen (Eds.), *Ancient superconti-
763 nents and the paleogeography of the earth*. Elsevier.
- 764 Evans, D. A. D., & Pisarevsky, S. A. (2008). Plate tectonics on early Earth? weigh-
765 ing the paleomagnetic evidence. *Geological Society of America Special Papers*,
766 440, 249–263. doi: 10.1130/2008.2440(12)
- 767 Fairchild, L. M., Swanson-Hysell, N. L., Ramezani, J., Sprain, C. J., & Bowring,
768 S. A. (2017). The end of Midcontinent Rift magmatism and the paleogeogra-
769 phy of Laurentia. *Lithosphere*, 9(1), 117–133. doi: 10.1130/L580.1
- 770 Feinberg, J., Solheid, P., Swanson-Hysell, N., Jackson, M., & Bowles, J. (2015).
771 Full vector low-temperature magnetic measurements of geologic materials.
772 *Geochemistry, Geophysics, Geosystems*, 16, 301–314. doi: 2014GC005591
- 773 Fisher, N. I., Lewis, T., & Embleton, B. J. J. (1987). *Statistical analysis of spherical*
774 *data*. Cambridge University Press. doi: 10.1017/CBO9780511623059

- 775 Gala, M. G., Symons, D. T. A., & Palmer, H. C. (1995). Paleomagnetism of the
 776 Jan Lake Granite, Trans-Hudson Orogen. *Saskatchewan Geological Survey*
 777 *Summary of Investigations, 95-4.*
- 778 Gower, C. F., Ryan, A. B., & Rivers, T. (1990). Mid-Proterozoic Laurentia-Baltica:
 779 An overview of its geological evolution and a summary of the contributions
 780 made by this volume. In C. F. Gower, T. Rivers, & A. B. Ryan (Eds.), *Mid-*
 781 *Proterozoic Laurentia-Baltica*. Geological Association of Canada, Special
 782 Paper.
- 783 Grove, M., & Harrison, T. M. (1996). $^{40}\text{Ar}^*$ diffusion in Fe-rich biotite. *American*
 784 *Mineralogist*, 81, 940–951. doi: 10.2138/am-1996-7-816
- 785 Hanson, G. (1968). K-Ar ages for hornblende from granites and gneisses and for
 786 basaltic intrusives in Minnesota. *Minnesota Geological Survey Report of Inves-*
 787 *tigations*, 8.
- 788 Harrison, T. M. (1982). Diffusion of ^{40}Ar in hornblende. *Contributions to Mineralogy*
 789 and Petrology, 78(3), 324–331. doi: 10.1007/BF00398927
- 790 Hodgskiss, M. S., Dagnaud, O. M., Frost, J. L., Halverson, G. P., Schmitz, M. D.,
 791 Swanson-Hysell, N. L., & Sperling, E. A. (2019). New insights on the Orosirian
 792 carbon cycle, early cyanobacteria, and the assembly of Laurentia from the
 793 Paleoproterozoic Belcher Group. *Earth and Planetary Science Letters*, 520,
 794 141–152. doi: 10.1016/j.epsl.2019.05.023
- 795 Hoffman, P. F. (1988). United plates of America, the birth of a craton: Early Pro-
 796 terozoic assembly and growth of Laurentia. *Annual Review of Earth and Plan-*
 797 *etary Sciences*, 16(1), 543–603. doi: 10.1146/annurev.ea.16.050188.002551
- 798 Hoffman, P. F. (1997). Tectonic genealogy of North America. In B. van der Pluijm
 799 & S. Marshak (Eds.), *Earth structure: An introduction to structural geology*
 800 and tectonics
- (p. 459–464). McGraw-Hill.
- 801 Holm, D. K., Anderson, R., Boerboom, T., Cannon, W., Chandler, V., Jirsa,
 802 M., ... Van Schmus, W. (2007). Reinterpretation of Paleoproterozoic ac-
 803 cretionary boundaries of the north-central United States based on a new
 804 aeromagnetic-geologic compilation. *Precambrian Research*, 157(1–4), 71–79.
 805 doi: 10.1016/j.precamres.2007.02.023
- 806 Holm, D. K., Darrah, K. S., & Lux, D. R. (1998). Evidence for widespread approx-
 807 imately 1760 Ma metamorphism and rapid crustal stabilization of the early

- 808 Proterozoic (1870-1820 Ma) Penokean Orogen, Minnesota. *American Journal*
809 *of Science*, 298(1), 60–81. doi: 10.2475/ajs.298.1.60
- 810 Holm, D. K., Gordon Medaris, L., McDannell, K. T., Schneider, D. A., Schulz, K.,
811 Singer, B. S., & Jicha, B. R. (2019). Growth, overprinting, and stabilization
812 of Proterozoic Provinces in the southern Lake Superior region. *Precambrian*
813 *Research*. doi: 10.1016/j.precamres.2019.105587
- 814 Holm, D. K., & Lux, D. R. (1996). Core complex model proposed for gneiss
815 dome development during collapse of the Paleoproterozoic Penokean oro-
816 gen, Minnesota. *Geology*, 24(4), 343. doi: 10.1130/0091-7613(1996)024<0343:
817 ccmpfg>2.3.co;2
- 818 Holm, D. K., Schneider, D., & Coath, C. D. (1998). Age and deformation of Early
819 Proterozoic quartzites in the southern Lake Superior region: Implications for
820 extent of foreland deformation during final assembly of Laurentia. *Geology*,
821 26(10), 907. doi: 10.1130/0091-7613(1998)026<0907:aadoep>2.3.co;2
- 822 Holm, D. K., & Selverstone, J. (1990). Rapid growth and strain rates inferred from
823 synkinematic garnets, Penokean orogeny, Minnesota. *Geology*, 18(2), 166. doi:
824 10.1130/0091-7613(1990)018<0166:rgasri>2.3.co;2
- 825 Holm, D. K., Van Schmus, W. R., MacNeill, L. C., Boerboom, T. J., Schweitzer, D.,
826 & Schneider, D. (2005). U-Pb zircon geochronology of Paleoproterozoic plu-
827 tons from the northern midcontinent, USA: Evidence for subduction flip and
828 continued convergence after geon 18 Penokean orogenesis. *Geological Society of*
829 *America Bulletin*, 117(3), 259–275. doi: 10.1130/b25395.1
- 830 Horan, M. F., Hanson, G. N., & Spencer, K. J. (1987). Pb and Nd isotope and
831 trace element constraints on the origin of basic rocks in an early Proterozoic
832 igneous complex, Minnesota. *Precambrian Research*, 37(4), 323–342. doi:
833 10.1016/0301-9268(87)90081-7
- 834 Irving, E. (2004). Early Proterozoic geomagnetic field in western Laurentia: im-
835 plications for paleolatitudes, local rotations and stratigraphy. *Precambrian Re-*
836 *search*, 129(3-4), 251–270. doi: 10.1016/j.precamres.2003.10.002
- 837 Jirsa, M., Boerboom, T., & Chandler, V. (2012). S-22, *Geologic Map of Minnesota,*
838 *Precambrian Bedrock Geology* (Tech. Rep.). Minnesota Geological Survey.
- 839 Karlstrom, K. E., Ahall, K.-I., Harlan, S. S., Williams, M. L., McLellan, J., &
840 Geissman, J. W. (2001). Long-lived (1.8-1.0 Ga) convergent orogen in

- southern Laurentia, its extensions to Australia and Baltica, and implications for refining Rodinia. *Precambrian Research*, 111(1-4), 5–30. doi: 10.1016/S0301-9268(01)00154-1
- Kissin, S. A., & Scott, S. D. (1982). Phase relations involving pyrrhotite below 350°C. *Economic Geology*, 77(7), 1739–1754. doi: 10.2113/gsecongeo.77.7.1739
- Ludwig, K. (1998). On the treatment of concordant uranium-lead ages. *Geochimica Cosmochimica Acta*, 62, 665–676.
- Medaris, L. G., Singer, B. S., Jicha, B. R., Malone, D. H., Schwartz, J. J., Stewart, E. K., ... Reiners, P. W. (2021). Early Mesoproterozoic evolution of midcontinental Laurentia: Defining the geon 14 Baraboo orogeny. *Geoscience Frontiers*, 12(5), 101174. doi: 10.1016/j.gsf.2021.101174
- Meert, J. G., Pivarunas, A. F., Evans, D. A., Pisarevsky, S. A., Pesonen, L. J., Li, Z.-X., ... Salminen, J. M. (2020). The magnificent seven: A proposal for modest revision of the quality index. *Tectonophysics*, 790, 228549. doi: 10.1016/j.tecto.2020.228549
- Mitchell, R. N., Bleeker, W., van Breemen, O., Lecheminant, T. N., Peng, P., Nilsson, M. K. M., & Evans, D. A. D. (2014). Plate tectonics before 2.0 Ga: Evidence from paleomagnetism of cratons within supercontinent Nuna. *American Journal of Science*, 314(4), 878–894. doi: 10.2475/04.2014.03
- Mutch, E. J. F., Blundy, J. D., Tatttich, B. C., Cooper, F. J., & Brooker, R. A. (2016). An experimental study of amphibole stability in low-pressure granitic magmas and a revised Al-in-hornblende geobarometer. *Contributions to Mineralogy and Petrology*, 171(10). doi: 10.1007/s00410-016-1298-9
- Park, J. K., Irving, E., & Donaldson, J. A. (1973). Paleomagnetism of the Precambrian Dubawnt Group. *Geological Society of America Bulletin*, 84(3), 859–870. doi: 10.1130/0016-7606(1973)84<859:potpdg>2.0.co;2
- Pehrsson, S. J., Eglington, B. M., Evans, D. A. D., Huston, D., & Reddy, S. M. (2015). Metallogeny and its link to orogenic style during the Nuna supercontinent cycle. *Geological Society, London, Special Publications*, 424, 83–94. doi: 10.1144/SP424.5
- Raub, T. M. (2008). *Paleomagnetism of Dubawnt Supergroup, Baker Lake Basin, Nunavut, Canada: Refining Laurentia's Paleoproterozoic apparent polar wan-*

- 874 *der path* (Unpublished doctoral dissertation). Yale University.
- 875 Rothstein, D. A., & Manning, C. E. (2003). Geothermal gradients in continental
876 magmatic arcs; constraints from the eastern Peninsular Ranges Batholith,
877 Baja California, Mexico. *Tectonic evolution of northwestern Mexico and the*
878 *Southwestern USA, Geological Society of America Special Paper*, 374. doi:
879 10.1130/0-8137-2374-4.337
- 880 Salminen, J., Pesonen, L. J., Mertanen, S., Vuollo, J., & Airo, M.-L. (2009). Palaeo-
881 magnetism of the Salla Diabase Dyke, northeastern Finland, and its implica-
882 tion for the Baltica-Laurentia entity during the Mesoproterozoic. *Geological*
883 *Society, London, Special Publications*, 323(1), 199-217. doi: 10.1144/SP323.9
- 884 Schmitz, M., Southwick, D., Bickford, M., Mueller, P., & Samson, S. (2018).
885 Neoarchean and Paleoproterozoic events in the Minnesota River Valley
886 subprovince, with implications for southern Superior craton evolution
887 and correlation. *Precambrian Research*, 316, 206–226. doi: 10.1016/
888 j.precamres.2018.08.010
- 889 Schoene, B., & Bowring, S. A. (2007). Determining accurate temperature-time
890 paths from U-Pb thermochronology: An example from the Kaapvaal craton,
891 southern Africa. *Geochimica et Cosmochimica Acta*, 71(1), 165–185. doi:
892 10.1016/j.gca.2006.08.029
- 893 Schulz, K. J., & Cannon, W. F. (2007). The Penokean orogeny in the Lake Superior
894 region. *Precambrian Research*, 157(1-4), 4–25. doi: 10.1016/j.precamres.2007
895 .02.022
- 896 Shankar, R., Sarma, D. S., Babu, N. R., & Parashuramulu, V. (2018). Paleomag-
897 netic study of 1765 Ma dyke swarm from the Singhbhum Craton: Implications
898 to the paleogeography of India. *Journal of Asian Earth Sciences*, 157, 235–244.
899 doi: 10.1016/j.jseaes.2017.08.026
- 900 Skipton, D. R., St-Onge, M. R., Schneider, D. A., & McFarlane, C. R. M. (2016).
901 Tectonothermal evolution of the middle crust in the Trans-Hudson Orogen,
902 Baffin Island, Canada: Evidence from petrology and monazite geochronology
903 of sillimanite-bearing migmatites. *Journal of Petrology*, 57(8), 1437–1462. doi:
904 10.1093/petrology/egw046
- 905 Smye, A., Marsh, J., Vermeesch, P., Garber, J., & Stockli, D. (2018, sep). Ap-
906 plications and limitations of U-Pb thermochronology to middle and lower

- 907 crustal thermal histories. *Chemical Geology*, 494, 1–18. doi: 10.1016/
908 j.chemgeo.2018.07.003
- 909 Southwick, D. L., Morey, G. B., & Mossler, J. H. (1986). Fluvial origin of the lower
910 proterozoic sioux quartzite, southwestern minnesota. *GSA Bulletin*, 97(12),
911 1432–1441. doi: 10.1130/0016-7606(1986)97<1432:FOOTLP>2.0.CO;2
- 912 Stauffer, M. R. (1984). Manikewan: An early Proterozoic ocean in central Canada,
913 its igneous history and orogenic closure. *Precambrian Research*, 25(1), 257–
914 281. doi: 10.1016/0301-9268(84)90036-6
- 915 Swanson-Hysell, N. L. (2021). The Precambrian Paleogeography of Laurentia. In
916 L. J. Pesonen, D. A. D. Evans, S. Å. Elming, J. M. Salminen, & T. Veikko-
917 lainen (Eds.), *Ancient supercontinents and the paleogeography of the earth*.
918 Elsevier.
- 919 Swanson-Hysell, N. L., Hoaglund, S. A., Crowley, J. L., Schmitz, M. D., Zhang,
920 Y., & Miller, J. D. (2020). Rapid emplacement of massive Duluth Com-
921 plex intrusions within the North American Midcontinent Rift. *Geology*. doi:
922 10.1130/g47873.1
- 923 Swanson-Hysell, N. L., Ramezani, J., Fairchild, L. M., & Rose, I. R. (2019). Failed
924 rifting and fast drifting: Midcontinent Rift development, Laurentia's rapid
925 motion and the driver of Grenvillian orogenesis. *GSA Bulletin*, 131, 913–940.
926 doi: 10.1130/b31944.1
- 927 Symons, D. T. A., & Harris, M. J. (2005). Accretion history of the Trans-Hudson
928 Orogen in Manitoba and Saskatchewan from paleomagnetism. *Canadian Jour-
929 nal of Earth Sciences*, 42(4), 723–740. doi: 10.1139/e04-090
- 930 Symons, D. T. A., Symons, T., & Lewchuk, M. (2000). Paleomagnetism of
931 the Deschambault pegmatites: Stillstand and hairpin at the end of the
932 Paleoproterozoic Trans-Hudson Orogeny, Canada. *Physics and Chem-
933 istry of the Earth, Part A: Solid Earth and Geodesy*, 25(5), 479–487. doi:
934 10.1016/s1464-1895(00)00074-0
- 935 Tauxe, L., Shaar, R., Jonestrask, L., Swanson-Hysell, N., Minnett, R., Koppers, A.,
936 ... Fairchild, L. (2016). PmagPy: Software package for paleomagnetic data
937 analysis and a bridge to the Magnetics Information Consortium (MagIC)
938 Database. *Geochemistry, Geophysics, Geosystems*, 17, 2450-2463. doi:
939 10.1002/2016GC006307

- 940 Thébault, E., Finlay, C. C., Beggan, C. D., Alken, P., Aubert, J., Barrois, O., ...
941 Zvereva, T. (2015). International Geomagnetic Reference Field: the 12th
942 generation. *Earth, Planets and Space*, 67(1). doi: 10.1186/s40623-015-0228-9
- 943 Van der Voo, R. (1990, 11 10). The reliability of paleomagnetic data. *Tectono-*
944 *physics*, 184(1), 1–9. doi: 10.1016/0040-1951(90)90116-P
- 945 Vermeesch, P. (2018). IsoplotR: A free and open toolbox for geochronology. *Geo-*
946 *science Frontiers*, 9(5), 1479–1493. doi: 10.1016/j.gsf.2018.04.001
- 947 Verwey, E. J. W. (1939). Electronic conduction of magnetite (Fe_3O_4) and its transi-
948 tion point at low temperatures. *Nature*, 144, 327–328. doi: 10.1038/144327b0
- 949 Weller, O. M., & St-Onge, M. R. (2017). Record of modern-style plate tectonics in
950 the Palaeoproterozoic Trans-Hudson orogen. *Nature Geoscience*, 10, 305–311.
951 doi: 10.1038/ngeo2904
- 952 Whitmeyer, S., & Karlstrom, K. (2007). Tectonic model for the Proterozoic growth
953 of North America. *Geosphere*, 3(4), 220–259. doi: 10.1130/GES00055.1
- 954 Xu, H., Yang, Z., Peng, P., Meert, J. G., & Zhu, R. (2014). Paleo-position of
955 the North China craton within the supercontinent Columbia: Constraints
956 from new paleomagnetic results. *Precambrian Research*, 255, 276–293. doi:
957 10.1016/j.precamres.2014.10.004
- 958 Zhang, S., Li, Z.-X., Evans, D. A. D., Wu, H., Li, H., & Dong, J. (2012). Pre-
959 Rodinia supercontinent Nuna shaping up: A global synthesis with new pale-
960 omagnetic results from North China. *Earth and Planetary Science Letters*,
961 353–354, 145–155. doi: 10.1016/j.epsl.2012.07.034

Table 1. Summary of site level paleomagnetic data

site	site lat	site lon	n	dec	inc	k	R	α_{95}	VGP lat	VGP lon
<i>northeast-trending dike magnetite-component site means</i>										
NED1	45.53423	265.75804	8	157.6	74.7	380	7.98	2.8	18.4	276.9
NED2	45.53421	265.75816	8	172.3	74.9	420	7.98	2.7	17.4	269.6
NED5	45.53309	265.75803	6	170.3	79.0	213	5.98	4.6	24.5	269.6
NED6	45.53299	265.75773	9	197.8	73.6	183	8.96	3.8	16.1	256.5
NED7	45.53288	265.75767	5	266.3	81.3	204	4.98	5.4	42.0	242.6
NED8	45.53286	265.75782	7	202.6	78.6	423	6.99	2.9	24.8	256.6
NED9	45.53314	265.75855	7	191.1	71.5	90	6.93	6.4	12.2	259.5
NED10	45.53259	265.75742	6	199.7	73.3	324	5.98	3.7	15.8	255.4
NED11	45.53252	265.75768	7	166.1	75.1	391	6.98	3.1	18.1	272.6
NED12	45.53489	265.76076	6	179.5	73.0	374	5.99	3.5	14.1	266.0
NED13	45.53497	265.76113	7	169.1	73.9	199	6.97	4.3	15.9	271.4
NED14	45.53492	265.76119	6	193.0	70.0	217	5.98	4.6	10.1	258.0
NED15	45.53688	265.76758	8	175.8	77.7	604	7.99	2.3	22.0	267.6
NED16	45.53728	265.76822	5	185.1	78.6	449	4.99	3.6	23.6	263.7
NED18	45.53124	265.76945	6	134.7	81.7	159	5.97	5.3	33.2	279.5
NED23	45.53398	265.74200	7	193.0	76.4	411	6.99	3.0	20.2	259.7
NED25	45.53396	265.74119	4	135.4	80.7	334	3.99	5.0	31.5	280.6
NED26	45.53445	265.74129	5	151.1	73.4	572	4.99	3.2	17.4	280.8
NED28	45.53467	265.73817	4	157.8	73.8	145	3.98	7.7	16.9	277.2
NED29	45.53438	265.73690	8	219.0	76.7	119	7.94	5.1	24.4	248.6
NED31	45.53385	265.75785	3	184.7	69.4	1730	3.00	3.0	8.7	262.9
NED34	45.51700	265.78083	8	185.9	77.0	362	7.98	2.9	20.8	263.1
NED35	45.53320	265.75761	8	166.4	74.7	261	7.97	3.4	17.4	272.6
mean pole: pole longitude: 265.8; pole latitude: 20.4; A_{95}: 4.5; K: 45.6 N: 23										
<i>northwest-trending dike magnetite-component site mean</i>										
NWD1	45.53407	265.76852	9	293.4	41.6	66	8.88	6.4	32.9	177.5

Notes: site lat–latitude of site ($^{\circ}$; WGS84); site lon–longitude of site ($^{\circ}$; WGS84) n–number of samples analyzed and included in the site mean; dec–tilt-correction mean declination for the site; inc–tilt-correction mean inclination for the site; k–Fisher precision parameter; R–resultant vector length; α_{95} –95% confidence limit in degrees; VGP lat–latitude of the virtual geomagnetic pole for the site; VGP lon–longitude of the virtual geomagnetic pole for the site.

Table 2. Summary of ID-TIMS $^{207}\text{Pb}/^{206}\text{Pb}$ East-Central Minnesota Batholith zircon dates

Sample	Unit	Latitude	$^{207}\text{Pb}/^{206}\text{Pb}$	Uncertainty (2σ)	MSWD	n/N
		Longitude	date (Ma)	X	Z	
ECMB6	St. Cloud Granite	45.53396° N 94.23187° W	1781.44	0.51	2.4	1.24
QP1	quartz-feldspar porphyry dike	45.53481° N 94.25811° W	1780.78	0.45	2.4	0.53
ECMB4	Richmond Granite	45.44343° N 94.48360° W	1776.76	0.49	2.4	1.15
						7/8

Notes: X is 2σ analytical uncertainty; Z is 2σ uncertainty including decay constant uncertainty. This Z uncertainty needs to be utilized when comparing to dates using other decay systems (e.g., $^{40}\text{Ar}/^{39}\text{Ar}$, $^{187}\text{Re}-^{187}\text{Os}$); MSWD is the mean squared weighted deviation; n is the number of individual zircon dates included in the calculated sample mean date; N is the number of individual zircons analyzed for the sample.